1 OF 1
AD
A058458

AFAL-TR-77-156
VOLUME II

LEVEL II $\bigcirc{2}$ NW

VARIABLE ACUITY DISPLAY DEVELOPMENT
VOLUME II : INFRARED LENS FEASIBILITY STUDY

MCDONNELL AIRCRAFT COMPANY
MCDONNELL DOUGLAS CORPORATION
P.O. BOX 516
ST. LOUIS, MO. 63166

August 1977

FINAL REPORT

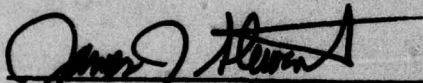APPROVED FOR PUBLIC RELEASE; DISTRIBUTION UNLIMITED.

78 155 088 00721

AIR FORCE AVIONICS LABORATORY
AIR FORCE WRIGHT AERONAUTICAL LABORATORIES
AIR FORCE SYSTEMS COMMAND
WRIGHT-PATTERSON AIR FORCE BASE, OHIO 45433

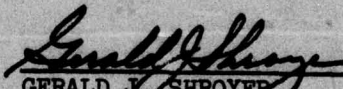JAMES J. STEWART
Project Engineer

GERALD J. SHROYER
Chief, Thermal Imaging Group

FOR THE COMMANDER

WILLIAM A. WALLACE, Lt Col, USAF
Chief, Electro-Optics & Reconnaissance
  Branch
Reconnaissance & Weapon Delivery Division

REPORT DOCUMENTATION PAGE

READ INSTRUCTIONS
BEFORE COMPLETING FORM

1. REPORT NUMBER	2. GOVT ACCESSION NO.	3. RECIPIENT'S CATALOG NUMBER
AFAL-TR-77-156 - Volume II VOL-2		

4. TITLE (and Subtitle)

VARIABLE ACUITY DISPLAY DEVELOPMENT.
Volume II. Infrared Lens Feasibility Study.

5. TYPE OF REPORT & PERIOD COVERED

FINAL TECHNICAL REPORT.

6. PERFORMING ORG. REPORT NUMBER

7. AUTHOR(s)

R.W. Fisher, R. Helmick, G. Licis
A. Rosenfeld

8. CONTRACT OR GRANT NUMBER(s)

F33615-76-C-1031 new

9. PERFORMING ORGANIZATION NAME AND ADDRESS

McDonnell Aircraft Company
McDonnell Douglas Corporation
P.O. Box 516, St. Louis, MO   63166

10. PROGRAM ELEMENT, PROJECT, TASK AREA & WORK UNIT NUMBERS

Project 2004/06/06

62204F

11. CONTROLLING OFFICE NAME AND ADDRESS

Air Force Avionics Laboratory
AFAL/RWI Vincent E. Diehl
Wright-Patterson AFB, Ohio   45433

12. REPORT DATE

August 1977

13. NUMBER OF PAGES

78

14. MONITORING AGENCY NAME & ADDRESS(if different from Controlling Office)

78p.

15. SECURITY CLASS. (of this report)

Unclassified

15a. DECLASSIFICATION/DOWNGRADING SCHEDULE

16. DISTRIBUTION STATEMENT (of this Report)

Approved for public release; distribution unlimited.

17. DISTRIBUTION STATEMENT (of the abstract entered in Block 20, if different from Report)

18. SUPPLEMENTARY NOTES

19. KEY WORDS (Continue on reverse side if necessary and identify by block number)

Infrared Lens   Displays
Variable Acuity   Vision
Optics   Narcissus

which

78 15 08 072

20. ABSTRACT (Continue on reverse side if necessary and identify by block number)

The feasibility of designing a nonlinear lens capable of operating with second generation infrared monolithic focal plane detector arrays has been established. The feasibility was based on a computer performance model while evaluated the effect of 3 to 5 micron or 8 to 14 micron infrared imaging spectrum, the number of scan lines, F/number, lens blur, and scanner type. In addition, the effects of narcissus were determined which resulted in requirements on lens element location.

DD FORM 1473   EDITION OF 1 NOV 65 IS OBSOLETE
1 JAN 73

403 111

20.   Abstract   (Continued)

The results indicate that such a lens could be built and should
operate in the 8 to 14 micron spectral region. It would have an
8 inch clear aperature and would have resolution and field-of-view
adequate to support human vision. In addition, it could be constructed
with state-of-art techniques and materials.

FOREWORD

This is Volume II of a two-volume final report of Contract No. F33615-76-C-1031. This volume covers the add-on effort to this contract. The objective of this add-on was to determine the feasibility of establishing the preliminary design and constructing a nonlinear lens capable of imaging in the infrared spectrum. The results of the study indicate that such a lens has a physical size consistent with its application to airborne FLIR systems and has resolution adequate to support human vision. It can be constructed with state-of-the-art materials and techniques.

TABLE OF CONTENTS

LIST OF ILLUSTRATIONS

Section 1

INTRODUCTION AND SUMMARY

This report documents the results and conclusions of the Add-On to Contract No. F33615-76-C-1031. The goal in this effort was to show the feasibility of constructing a nonlinear lens capable of imaging in the infrared wavelength spectrum. Except for wavelength of operation, this lens has optical characteristics similar to the existing visual spectrum nonlinear lens which was developed during a previous contract[1]*.

That lens takes advantage of the "variable acuity" characteristic of human vision to reduce the amount of information that must be transmitted in a wide field-of-view high resolution imaging system. A brief description of this concept is presented in Appendix A. A laboratory brassboard of that system was constructed under contract to the Office of Naval Research (ONR)[2] and is presently under final testing at MCAIR.

The system developed for ONR operates in the visual wavelength spectrum and consequently is usable only during daylight hours. The goal of this effort was to determine the feasibility of achieving the same wide field-of-view, high resolution capability during night-time hours by operating the sensing lens in the infrared wavelength spectrum. If successful, this sensor system could fully support human vision under clear night conditions; a capability impossible to achieve with conventional FLIR imaging systems.

A brief description of this effort and the results are now presented. A flow diagram of the overall effort is shown in Figure 1. It consists of two phases, an analysis phase and a design phase. In the analysis phase, the optimum parameters and constraints are determined that are necessary for the actual lens design effort which will be accomplished in the design phase.

A computer controlled optimization analysis indicated that the lens should be designed as an F/2.0 with an optical quality represented by a point spread function in the focal plane which has a one sigma width (radius) of 16 microns. The best operating region was found to be 8-14 microns.

A narcissus analysis shown on Figure 1 was performed on the optical relay early in the effort to assist in establishing element curvatures and spacings of optical elements close to the focal plane. As the actual lens design evolved, the narcissus analysis was expanded to include those elements.

The lens design phase proved conclusively that an infrared nonlinear lens is feasible. It can be built with the required optical characteristics (F/2.0, 16 micron blur, 8-14 micron wavelength spectrum) and is of reasonable size (8 inch clear aperture maximum). Narcissus images were found to be well below the detector Noise Equivalent Power (NEP) when current generation scanners are used. However, when used with second generation monolithic focal plane array detectors, dynamic electronic compensation of detector outputs to reduce narcissus images to an acceptable level will be required because of the larger cold assembly area and anticipated better sensitivity.

* Number shown as superscript refers to the corresponding item in the List of References.

Optimization Analysis

Visual Lens Data

Scanner Data

NVL Model

Input Definition

Analytic Model Development

Parametric Analysis 8-14 μ Current Generation Det Technology

Accomplished under U.S. Navy contract

Parametric Analysis 8-14 μ Second Generation Det Technology

Parametric Analysis 3-5 μ Second Generation Det Technology

Study Integration and Optimum Parameter Selection

System Performance

Optical Parameters

Lens Design and Optimization

Relay Considerations

Optical Design

Narcissus Analysis

Basic IR Theory

Narcissus Analytic Model Development

Optical Relay Analysis

Nonlinear Lens Analysis

GP77-0292-2

FIGURE 1
ANALYSIS FLOW DIAGRAM

Section 2

ANALYSIS

The analysis portion of this effort proceeded along the lines shown on Figure 1. Basically it is divided into two separate efforts, the Optimization Analysis and the Narcissus Analysis. They were run in parallel which was dictated by the tight schedule for the supply of data required by the lens design effort.

The key portion of the analytic effort is the optimization effort. As shown on the figure this required the definition of all inputs, the development of computer programs, the performance of size/performance parameter tradeoffs, and integration of results to facilitate selection of the best nonlinear lens design parameters.

The narcissus analysis paralleled the optimization analysis so that guidelines for minimizing narcissus could be established for the lens design effort concurrent with the availability of other optical design parameters. Again refering to the flow diagram of Figure 1, this meant that the narcissus theory had to be developed, since none was available in sufficient detail. The goal of the first narcissus effort was to assess the contribution of the optical relay since this impacted on the rear element design of the nonlinear lens. After the lens design began to evolve, narcissus analysis was run on the lens to determine its contribution to narcissus image generation. Only minor changes to lens design to reduce narcissus was possible because of time and effort constraints. Details of these analyses are presented below.

2.1 OPTIMIZATION ANALYSIS

APPROACH

The overall objective of this effort is to establish the parameters for an infrared foveal lens design. Since specific mission requirements and/or state-of-the-art in infrared variable acuity technology are not defined at this time, the approach selected was a computerized optimization which allowed interactive variation of key parameters while size and performance were assessed. An optimum size/performance balance was achieved and a lens was preliminarily designed for these optimum parameters. A flow diagram of this approach is shown in Figure 2.

Optimization philosophy is as follows: Experience from our visual lens work showed that lens size (linear dimensions) increase inversely with both optical quality (blur) and F/number. Conversely performance measured by Minimum Resolvable Temperature (MRT) improves directly with these two parameters. The approach shown on Figure 2 was developed to determine the best performance but with reasonable size.

Inputs for the study were

(a) Parameters from our existing visual spectrum lens

3

(b) Present and future scanner and detector parameters*
(c) System inputs

Study Inputs

Existing Lens
Characteristics
• Distortion
• FOV
• Fabrication
  Constraints

☐ Scanner
  Parameters
• Serial/Parallel
• Scan Efficiency
• Overscan Ratio

Detector
Parameters
Ⓝ Geometry
☐ D*, Response

☐ Variable Inputs
Ⓞ Trade-Off Parameters

Lens
Optical
Parametrics

L(O)

L (θ)

Image
Size

Optical
Relay
Parametrics

L_C/L_D

Performance
Calculations
NVL Model

Lens
Size
Parametrics

Size (σ, F_{no})

Blur
σ

F_{no}

MRT (f_X, θ, F_{no}, σ, N)

System Inputs

λ Wave Length
• Atmospheric Transmission
• Optical Transmission
• System Electronic Response
• Display Quality
• Magnification
• Frame Rate
• Eye Integration Time
• Temperature and Emissivity
• Vibration
• Threshold S/N

Optical
Design
Study

F_{no}, σ

Parametric
Analysis
and
Selection
• Min Size
• Min MRT
• Max f_X

Size and
MRT for
Recom-
mended
Systems

*Design
Parameters

GP77-0292-3

FIGURE 2
OPTIMIZATION ANALYSIS TECHNICAL APPROACH

In general, these inputs fall within three categories. These are constant
inputs that do not change in the study, variable inputs which were changed
discretely at various points during the studies, and tradeoff parameters
that were tested over a range of values to determine the effect of each on
performance and size. The latter are F/number and blur (previously discussed)
and the number of effective scan lines per picture height (N). This addi-
tional tradeoff parameter surfaces early in the study as a key parameter
because of its major influence on system resolution and the possibility of its
control in future detector development. The variable inputs are spectral
wavelength regions and scanner/detector parameters. The spectral wavelength
bands used in the study are in the 3-5 micron region and 8-14 micron regions.
Since these regions require different detectors, D* and electronic detector

4

response were changed when spectral band was changed. The other variable inputs are the scanner parameters which are established by present and future technology. A state-of-the-art serial scanner and a parallel scanner were evaluated separately[3]. However, the primary emphasis in this study was placed on the utilization of a second generation monolithic focal plane array scanner. Such a scanner was theorized in both spectral bands while the state-of-the-art scanners were studied in the long wavelength band only. The function of these inputs and the rationale' for their selection in the analysis are described below.

LENS OPTICAL PARAMETERS

Starting at the upper left of Figure 2, the optical requirements of distortion, field-of-view, and fabrication constraints are used to define focal length and image size requirements of the nonlinear lens. The basis for the selection of these inputs is as follows: (1) The amount of distortion used was made equal to the existing lens. This function provides a good match to human visual acuity and is believed to be near the maximum distortion technically possible. In addition, any sensing system constructed with this function will be compatible with the display systems constructed on related contracts. (2) A field-of-view (FOV) goal of 160° was utilized for the study. This value was selected because no significant reduction in either size or bandwidth is achieved for smaller 90°-100° fields-of-view. In addition this FOV does not impose any difficulty in design. (3) Fabrication of our existing visual spectrum lens has shown that the rear element spherics are extremely difficult to produce if the diameter is less than 0.75 inch.

The relationships established by these parameters are shown in Figure 3. These curves were used to select an on-axis focal length of 2 inches. This then established an image size of 0.72 inch for 160° coverage. A curve for a 100° FOV is also shown on Figure 3 to emphasize the point made above that little is gained through FOV reduction.

GP77-0292-6
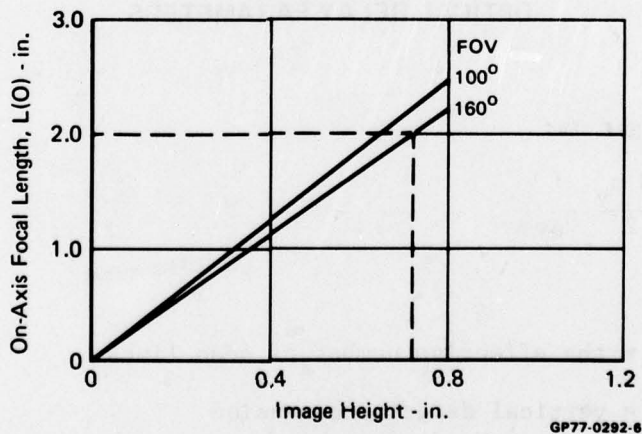
FIGURE 3
FOCAL LENGTH/IMAGE SIZE PARAMETRICS

*All analyses and results pertaining to current technology scanners was extracted from a related NAVY contract.[3]

OPTICAL RELAY PARAMETERS

When the image size is known, it is possible to define the optical relay that couples the image to the detector plane. The basic geometry for this is shown in Figure 4. The optical relay must be defined because it establishes how the nonlinear lens F/number appears to the detector (Figure 2) for sensitivity calculations and to establish how the detector dimensions translate to the lens focal plane (Figure 3), required for spatial frequency calculations. The required ratio (L_C/L_D) is the ratio of the nonlinear lens image size (H) to the effective detector scan plane height (H_D) (Figure 4). The lens image size is 0.36 inch. The effective detector height H_D depends on the detector assembly and scan technique used.

$$\frac{L_C}{L_D} = \frac{H}{H_D}$$
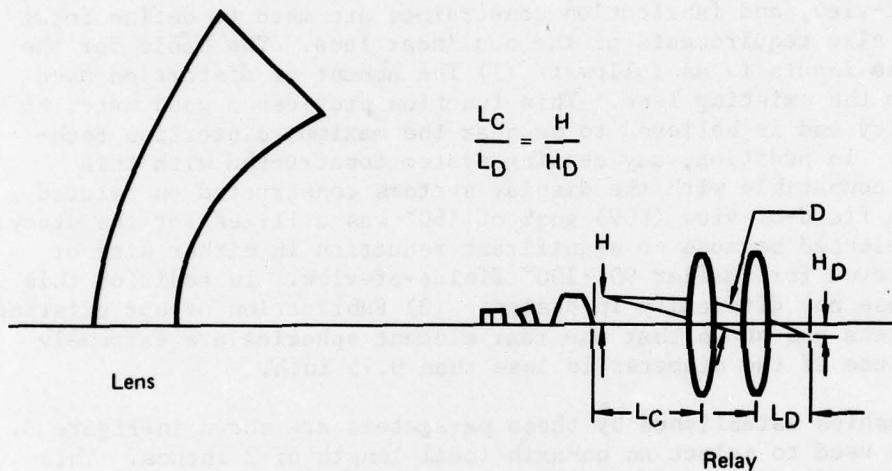
Lens

Relay

GP77-0292-4

FIGURE 4
OPTICAL RELAY PARAMETERS

In general this height is:

$$H_D = \frac{N\,a_y}{2}\,\eta_{ovsc}$$

(1)

where

N = the effective number of scan lines

a_y = vertical detector dimension

η_{ovsc} = line overscan ratio

Since the optics are collimated between the two lenses

$$\frac{H}{L_c} = \frac{H_D}{L_D} \tag{2}$$

Substituting Equation (2) and (1) and rewriting

$$\frac{L_D}{L_c} = \frac{N\, a_y\, \eta_{ovsc}}{2\, H} \tag{3}$$

The detector size (Δh_y) measured in the y direction and in the lens image plane is

$$\frac{\Delta h_y}{L_c} = \frac{a_y}{L_D} \tag{4}$$

Using the focal length ratio of Equation (3) and substituting into (4) results in

$$\Delta h_y = \frac{a_y\, L_c}{L_D} = \frac{2\, H}{N\, \eta_{ovsc}} \tag{5}$$

Note that Δh_y is independent of detector size. In the x direction, the detector size is

$$\Delta h_x = a_x\, \frac{L_c}{L_D} = \frac{2\, H}{N\, \eta_{ovsc}}\, \frac{a_x}{a_y} \tag{6}$$

If a_x and a_y are related by a constant (K)

$$\Delta h_x = \frac{2H\, K}{N\, \eta_{ovsc}} = K\, \Delta h_y \tag{7}$$

Since these increments are not dependent on detector size, the detector spatial MTF's will also be independent of detector size.

The F/number of the detector $(F\#_D)$ in terms of the nonlinear lens $(F\#)$ will now be developed from Figure 4. The ray bundle diameter (D) shown on Figure 4 is defined by

$$D = \frac{L_c}{F_\#} \tag{8}$$

The F/number $(F\#)$ of the nonlinear lens is also equal to the F/number of the relay $(F\#_C)$. The F/number of the detector $(F\#_D)$ is

7

$$F\#_D = \frac{L_d}{D} \tag{9}$$

Solving for D and setting Equation (9) equal to (8) results in

$$\frac{F\#_D}{F\#} = \frac{L_D}{L_c} \tag{10}$$

The F/number ratio in terms of scanner parameters may be defined by substituting Equation (3) into (10)

$$\frac{F\#_D}{F\#} = \frac{N\ a_y\ \eta_{ovsc}}{2\ H} \tag{11}$$

An interesting observation can be derived from this equation. From Reference (4) signal power falling on a single detector element is directly proportional to detector area (A_D) and inversely to detector F/number ($F\#_D$), viz.

$$P_D \sim \left(\frac{A_D}{F\#_D}\right)^2 \tag{12}$$

and since the detector area is

$$A_D = a_x\ a_y = K\ a_y^2 \tag{13}$$

Therefore

$$P_D \sim \left(\frac{a_y^2}{F\#_D}\right)^2 \tag{14}$$

If Equation (11) is used to express signal power in terms of nonlinear lens F/number ($F\#$) which is by definition also relay lens F/number ($F\#_c$)

$$P_D \sim \frac{4\ H^2}{N^2\ \eta_{ovsc}\ F\#^2} \tag{15}$$

If the image height (H) and overscan ratio (η) are constant we may write a proportionality

$$P_D \sim \frac{1}{N^2\ F\#^2} \tag{16}$$

8

Therefore signal power is not dependent on detector area but only on F/number and scan line count. In NVL[3] the noise power is proportional to the square root of detector area. The result is that the NEDT and, therefore, MRT are directly proportional to the square root of detector area. Therefore, the MRT is directly proportional to detector linear dimension if the detector remains symmetrical as its size varies. If the number of scan lines and nonlinear lens F/number remain constant, smaller detectors result in better performance. Since a simple linear relationship exists between performance and detector size, it was not retained as a tradeoff parameter for second generation detector analysis. Instead, the smallest detector dimension that was practical was used, viz.

$$a_x = a_y = 0.001 \text{ inch}$$

This leaves $F_\#$ and N as the only scanner related tradeoff parameters. $F_\#$ was varied from F/1.0 to F/11.0 and scan lines from 131 to 2000. For current generation scanners, detector sizes and N are fixed. Thus only $F_\#$ is a tradeoff parameter. These fixed values of detector size and N are shown in Figure 5.

Parameter	Serial	Parallel
N	488	360
a_x	0.0013 in.	0.002 in.
a_y	0.0015 in.	0.002 in.

GP77-0445-1

FIGURE 5
CURRENT GENERATION SCANNER PARAMETERS

Now the overscan ratio will be defined. The overscan ratio (η_{ovsc}) is the ratio of detector vertical subtense (Δh_y) to actual scan line spacing and may be defined by the equation:

$$\eta_{ovsc} = \frac{a_y \; L_c \; N}{2H \; L_D} \qquad (17)$$

To put a value on this parameter, the type of scanning to be used must be theorized. For the primary tradeoff analysis a second generation hybrid scan technique was used, i.e., a parallel array with serial time delay and integration (TDI). For these systems an overscan ratio of one was used. For the current generation scanners, the serial scanner used a ratio of 1.5 while the parallel scanner utilized a ratio equal to one.

9

In the second generation analyses, the number of serial detectors was always equal to nine. This number was based on customer inputs which stated that the payoff of using more than nine was questionable when such things as switching noise and relative image detector motion during TDI were considered. The current generation serial scanner also employed nine TDI detectors.

The remaining scanner parameters of D* was selected as follows: For 3-5 micron systems, InSb as a detector was assumed with a

$$D* = 5 \times 10^{11}$$

For the 8-14 micron system the same material was selected. The D* value is

$$D* = 5 \times 10^{10} \quad .$$

These values include improvements due to effective cold shielding. Manufacturer's actual improvement data was used to estimate the improvement rather than theoretical values. Detector equivalent electronic response BW was determined from the manufacturer's literature. This parameter was found to be significant only in the case of the serial scanner.

LENS SIZE PARAMETRICS

During initial phases of the study, the lens size parametrics, i.e., size as a function of F/number and optical blur of the existing visual spectrum lens was used. These parametrics are shown in Figure 6. As actual lens design progressed, these parametrics were updated. However, this was not found to be necessary. All optimized designs fit these data very accurately.

PERFORMANCE CALCULATIONS

System performance in terms of MRT was computed using the Night Vision Laboratory (NVL) FLIR model which was suitably modified for the VARVS system. This model and its modifications is described in Appendix B. Other than parameters previously discussed, this model required the parameters listed on Figure 7. The basis for selection of the more salient parameters is listed below.

(a) Wavelength Range - For both spectrums these were selected as regions of good atmospheric transmission over reasonable path lengths.

(b) Atmospheric transmission - Original plans were to use 0.5 but were changed to 1.0 to reflect system performance rather than the extremely variable mission performance.

(c) Optical transmission - Based on state-of-the-art coating techniques, a 0.5% reflectance for each of 10 elements (two surfaces each).
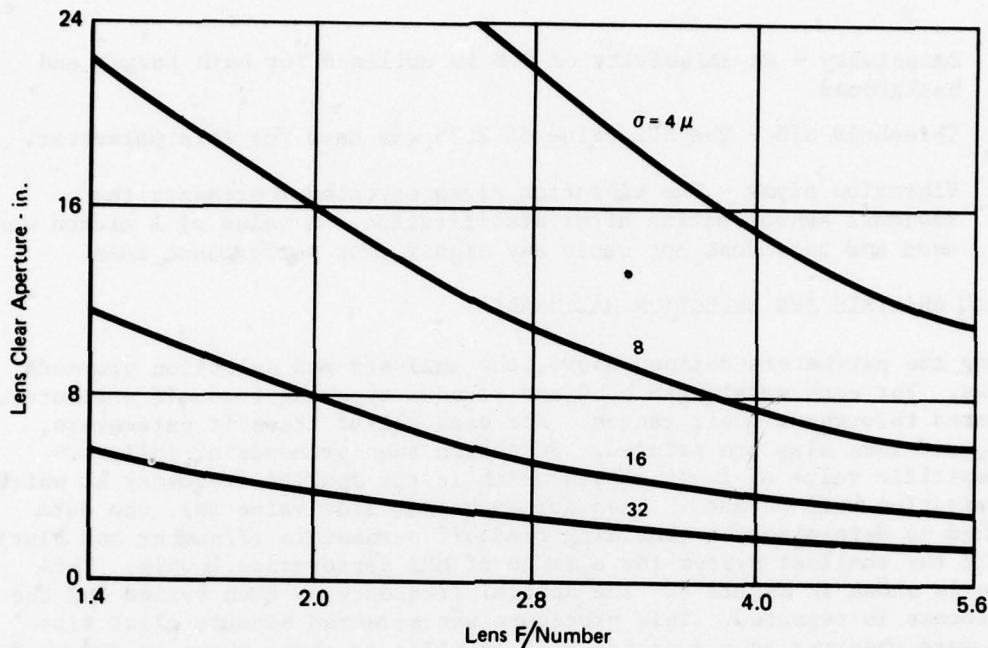
FIGURE 6
SIZE PARAMETRICS FOR A 2-IN. FOCAL LENGTH LENS

(d) (e) System electronic response – Since the NVL model includes no internal noise sources other than the detector, electrical response was made insignificant for all systems by assuming flat response out to the highest spactial frequency (f_x) of interest which was determined by $f_x > \dfrac{1}{2I_{FOV}}$, where I_{FOV} is the instantaneous FOV. This assumption is entirely adequate for the NVL model because (1) response is limited by detector geometry, and (2) noise bandwidth is limited by human observer factors such as eye integration time and the matched filter function (see Appendix B).

(f) Display blur – The characteristics of the direct view display were used for this parameter. This unit has a blur sigma in angular terms of 0.26 minutes arc. This is about 10 times better than the antici-pated system resolution. When utilizing the NVL model it was most convenient to convert this to linear spatial blur at the same focal length as the nonlinear lens which is 3.9 microns.

(g) Display magnification – The VARVS concept inherently has unity magnification.

(h) Frame rate – A TV compatible frame rate of 30 frames/second is uti-lized for all analyses with two fields per frame (2/1 interlace).

(i) Eye integration time – The NVL recommended value of 0.2 sec. was used for this parameter.

(j) Temperature – The usual 300°K value was used for nominal scene temperature.

11

(k) Emissivity - An emissivity of 0.8 is utilized for both target and background.

(l) Threshold S/N - The NVL value of 2.25 was used for this parameter.

(m) Vibration sigma - The vibration sigma selected represents the residual sensor motion after stabilization. A value of 1 micron was used and this does not cause any significant performance loss.

PARAMETRIC ANALYSIS AND SELECTION RATIONALE'

Using the parameters defined above, the analysis and selection proceeds as follows. For each wavelength band and scanner type the tradeoff parameters are iterated throughout their ranges. For each set of tradeoff parameters, MRT vs f_x and lens size are printed. Selection then proceeds as follows. First a specific value of f_x is chosen which is the spatial frequency at which the optimization will be made. Then for each scan line value (N), the data is screened to determine the remaining tradeoff parameters (F/number and blur) that yield the smallest system for a range of MRT performance levels. This procedure is shown in Figure 8. The spatial frequency is then varied and the entire process is repeated. This procedure was selected because clear size minimums were observed as a function of N, similar to those shown on Figure 8. These minimums were recorded along with their system parameters and used to plot size vs MRT for each spatial frequency of optimization as shown on the right of Figure 8. These data were used to locate the point where a reduction of MRT is not warranted by the corresponding increase in size. The knee points of the curves represent the best selection. Beyond these points, excessive size results with little improvement in MRT. Finally the MRT curves for the selected systems (one optimum for each design f_x) are plotted as shown on the lower right of Figure 8. A subjective choice is then made as to which is most acceptable from a mission performance and vehicle installation standpoint. The results of the analysis will now be presented.

RESULTS OF OPTIMIZATION ANALYSIS FOR SECOND GENERATION DETECTOR TECHNOLOGY

The second generation scanner size parametrics as a function of effective scan lines are shown in Figures 9 through 12 for the 3-5 micron spectrum and in Figures 13 through 16 for the 8-14 micron spectrum. Spatial frequencies of optimization are 0.3, 0.5, 0.7 and 1.0 cycle/mr. Separate figures are presented for each of these frequencies. Performance MRT values range from 0.05°C to 0.5°C. These ranges of both MRT and spatial frequency were chosen because they cover the anticipated requirements. Some comments on these data are:

(a) The 3-5 micron curves, Figures 9 through 12 are presented in order of increasing spatial frequency of optimization. Note how the optimum scan minimum size increases with spatial frequency of optimization with clear minimums occurring on Figures 11 and 12 (0.7 and 1.0 cycle/mr.)

(b) At any particular spatial frequency of optimization, minimums occur at the same scan frequency regardless of the MRT requirement.

12

Name	Units	Program Variable	Value: 2nd Gen Det System		Value: State of Art Systems Serial	Value: State of Art Systems Parallel
Nominal Wavelength Band	microns		3-5	8-14 ⟶		
Actual Wavelength Band Used	microns	LAM	3.4-4.2	8.5-13 ⟶		
Detector Type			InSb	HgCdTe ⟶		
D*		DSTAR	$5(10^{11})$	$5(10^{10})$ ⟶		
Detector Width	in.	AX	0.001	0.001	0.0013	0.002
Detector Height	in.	AY	0.001	0.001	0.0015	0.002
Half-Image Height on Nonlinear Lens Image Plane	in.	HMAX	0.36 ⟶			
Nonlinear Lens On-Axis Focal Length	in.	LO	2.0 ⟶			
Relay to Nonlinear Lens Focal Length Ratio	—	LRLS	$\dfrac{2\ ETA\ HMAX}{1.1\ AY\ XN}$			
Relay Focal Length	in.	LRLY	—	—	$\dfrac{HMAX}{TAN(\theta/2)}$	—
Relay F/Number	—	FNRLY	0	0	$\dfrac{LRLY}{EPD}$	0
F/Number Evaluated	—	FNO	1-11 ⟶			
Optics Transmission	—	TAUO	0.9 ⟶			
Magnification	—	MAG	1.0 ⟶			
Lens Blur (1σ) Evaluated	microns	Sigma	4-30 ⟶			
Entrance Pupil Diameter	in.	EPD	∞	∞	0.586	∞
Serial Detector No.	—	DETN	9	9	9	1
Detector Time Response BW	HZ	FSTAR	MTF=1 ⟶		$13(10^{6})$	MTF=1
Electronics BW	HZ	FO	MTF=1 ⟶			
Atmospheric Transmission	—	TAUA	1.0 ⟶			
Eye Signal to Noise Detection Threshold	—	SNR	2.25 ⟶			
Eye Integration Time	sec	TE	0.2 ⟶			
Total Scan Lines Evaluated	—	XL	131-2000	131-2000	525	480
Vertical Scan Efficiency	—	XKV	0.084	0.084	0.0705	—
Scan Velocity	in./sec	VX	$\dfrac{2\ HMAX\ FR}{1\text{-}XKV}$ ⟶		$\dfrac{2\ HMAX\ FR\ XN}{(1\text{-}XKV)(1\text{-}XKH)}$	$\dfrac{HMAX\ FR}{1\text{-}XKH}$
Horizontal Scan Efficiency	—	XKH	—	—	0.1733	0.25
Overscan Ratio	—	ETA	1.0	1.0	1.5	1.0
Frame Rate	sec^{-1}	FR	30 ⟶			
Display Spot Size (1σ)	microns	SIGMAD	15.37 ⟶			

Notes:
XN is the effective number of scan lines, θ is the relay field-of-view angle

GP77-0328-13

FIGURE 7

PARAMETERS USED IN SYSTEM EVALUATION

13

- Compute MRT (f_X, F_{no}, σ, N)
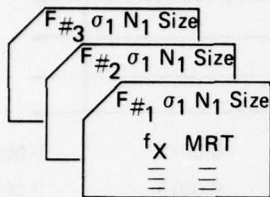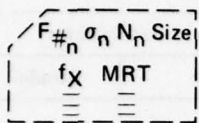
- For Selected f_X's Plot Size vs N for Specific MRT values*
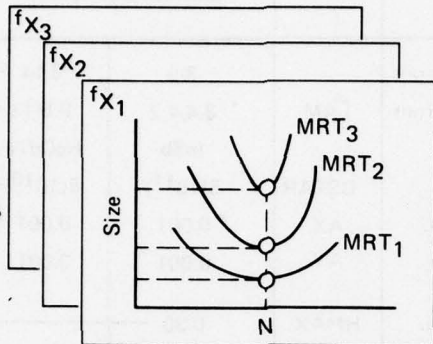
- Plot Minimum Size System for Each f_X/MRT Combination. Select Best Lens Parameters Based on ΔSize/ΔMRT

$F_{\#n}$ σ_n N_n Size

f_X MRT

$F_{\#3}$ σ_1 N_1 Size

$F_{\#2}$ σ_1 N_1 Size

$F_{\#1}$ σ_1 N_1 Size

f_X MRT

f_{X_3}

f_{X_2}

f_{X_1}

MRT₃ → MRT_3
MRT_2
MRT_1

Size

N

Minimum Size

f_{X_3}
f_{X_2}
f_{X_1}

MRT
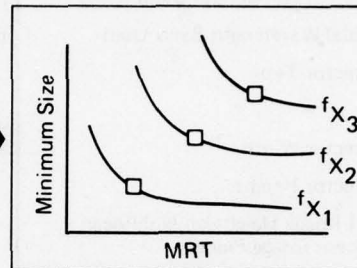
- Plot MRT Curves for Selected Optimum Systems

1 2 3

MRT

f_X
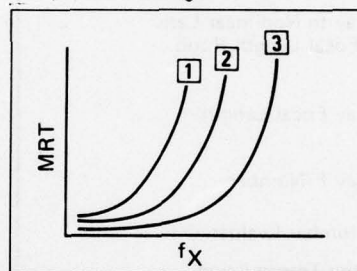
GP77-0292-7

*This step not necessary for current scanners where N is specified.

FIGURE 8
PARAMETRIC ANALYSIS AND SELECTION

MRT = 0.05°C   0.1°C

0.2°C

0.5°C

40

30

20

10

0

Diameter Clear Aperture - in.

0   400   800   1200   1600   2000

Effective TV Lines
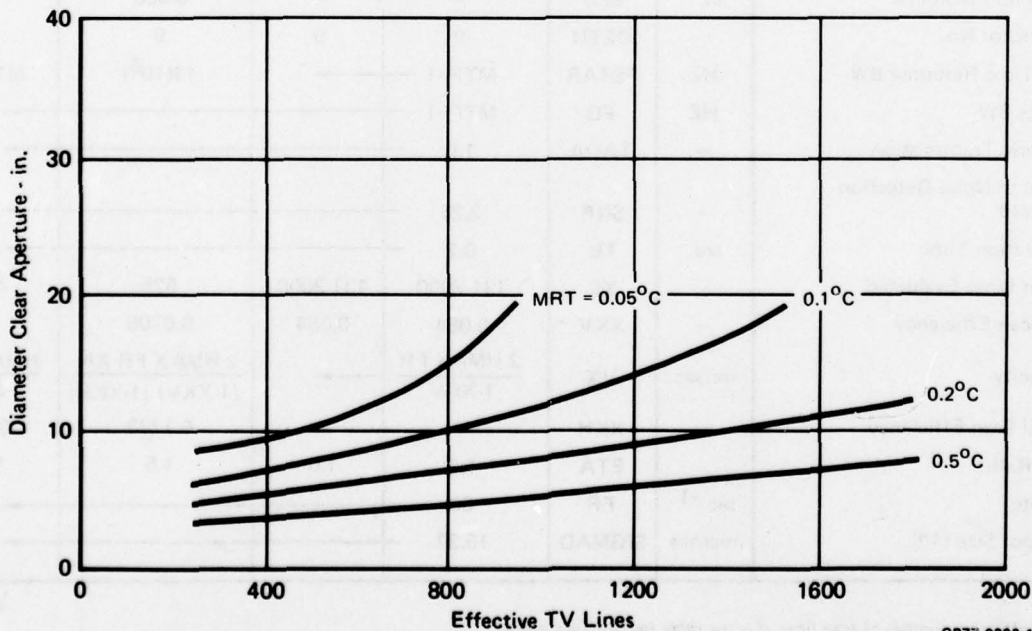
GP77-0292-11

FIGURE 9
2nd GENERATION DETECTOR LENS SIZE REQUIREMENTS
Wavelength: 3-5 μ Frequency: 0.5 c/mr

14

FIGURE 10
2nd GENERATION DETECTOR LENS SIZE REQUIREMENTS
Wavelength: 3-5 μ Frequency: 0.3 c/mr
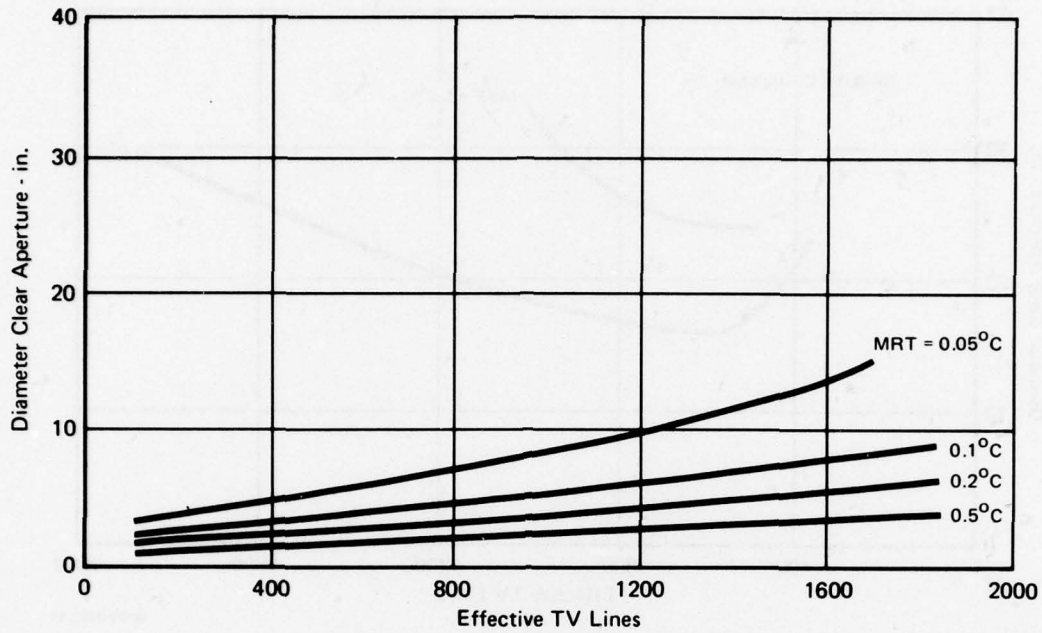
GP77-0292-8

FIGURE 11
2nd GENERATION DETECTOR LENS SIZE REQUIREMENTS
Wavelength: 3-5 μ Frequency: 0.7 c/mr
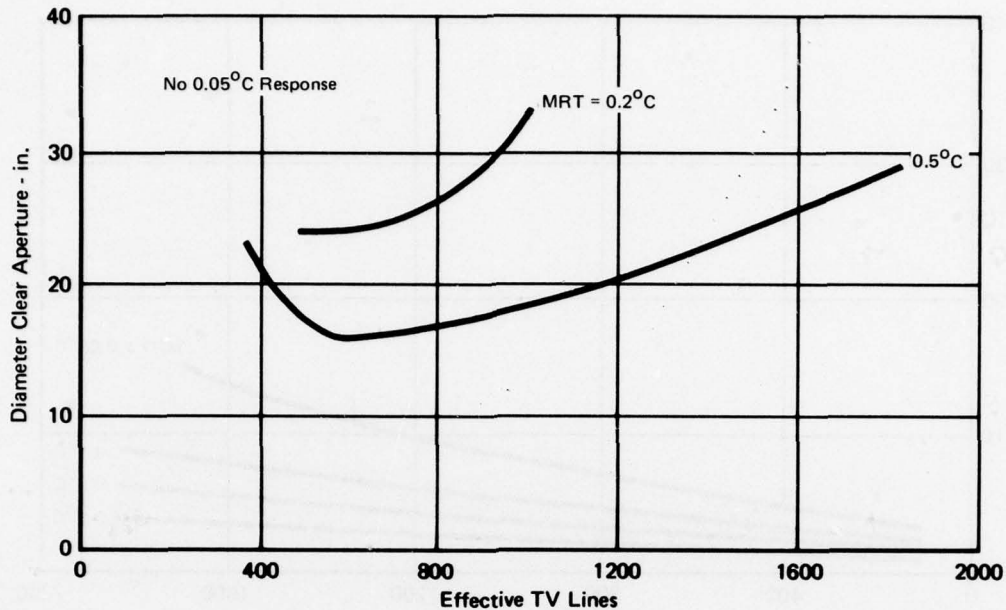
GP77-0292-10

FIGURE 12
2nd GENERATION DETECTOR LENS SIZE REQUIREMENTS
Wavelength: 3-5 μ Frequency: 1.0 c/mr

GP77-0292-17

(c) Trends in the 8-14 micron data on Figures 13 through 16 are approximately the same as for the 3-5 micron case. However, sizes are significantly lower for the same spatial frequency. This is clearly illustrated at the next step in optimization shown on Figure 17.

In Figure 17, line rate is eliminated as a variable by selecting the systems from the previous figures that have the optimum line rate (that which yields minimum size for the same performance). This curve is used to make the final tradeoffs between spectral regions and between size and performance. The former is clearly seen by comparing performance of systems of similar sizes. For example, if 0.7 c/mr spatial resolution is desired, an 8 inch diameter system would have a MRT of 0.12°C in the 8-14 micron spectral region and MRT of 0.3°C in the 3-5 micron spectral region. Another way of making the comparison is on a constant MRT performance basis. For example, if 0.1°C MRT is required at 0.7 cycle/mr, a 3-5 micron system would have a diameter of almost 14 inches while the 8-14 micron would have 8.5 inch diameter. Similar trends exist at all performance and size levels. Therefore, the 8-14 micron spectral region seems to be a clear choice.

The curves of Figure 17 can also be used to locate the best size or performance combination. This occurs at the knee of the curves where size starts increasing excessively while performance improves only slightly. These points are shown on Figure 18 for the six optimum systems (three spatial frequencies, two spectral regions). A description of these optimum systems is listed in Figure 19. A direct comparison of the performance of these six systems is presented in Figure 20. Here the MRT vs. spatial frequency is shown for each system. These curves show again the size advantages of the 8-14 micron region and

16

GP77-0292-16

FIGURE 13
2nd GENERATION DETECTOR LENS SIZE REQUIREMENTS
Wavelength: 8-14 μ Frequency: 0.3 c/mr

GP77-0292-15
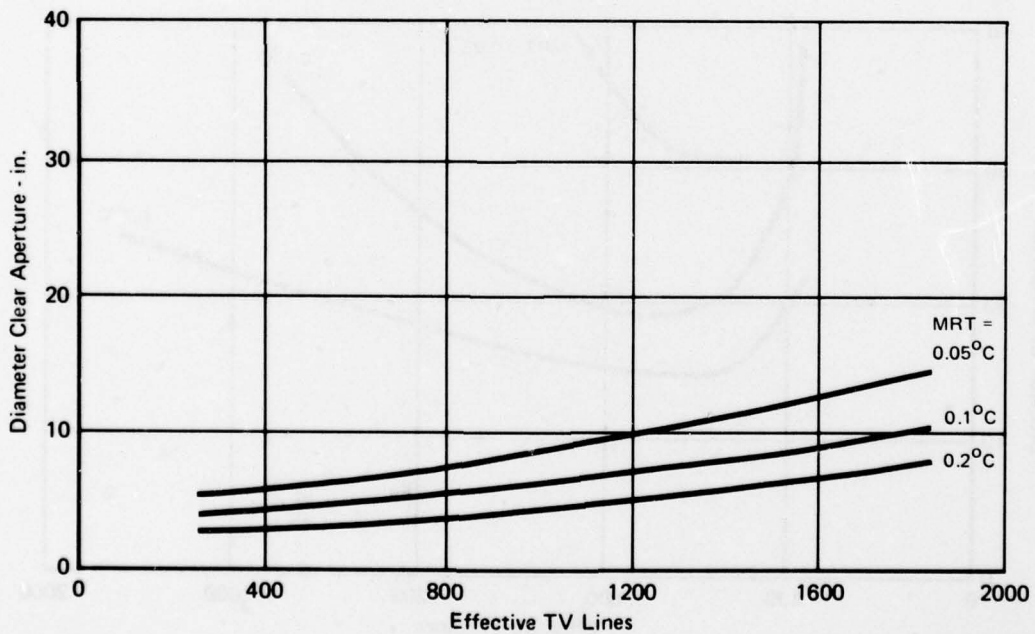
FIGURE 14
2nd GENERATION DETECTOR LENS SIZE REQUIREMENTS
Wavelength: 8-14 μ Frequency: 0.5 c/mr
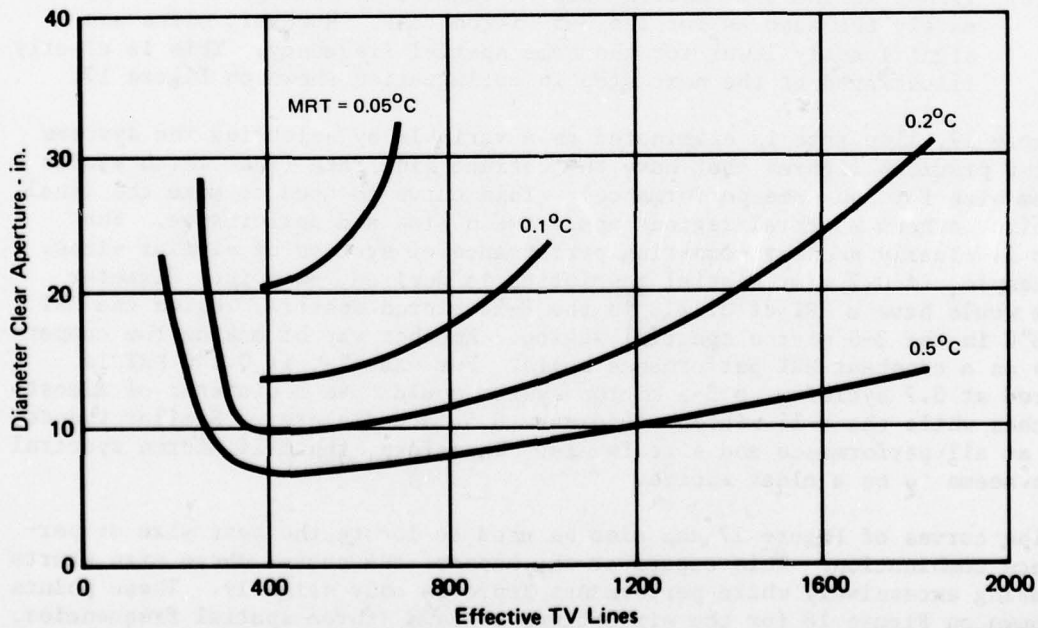
17
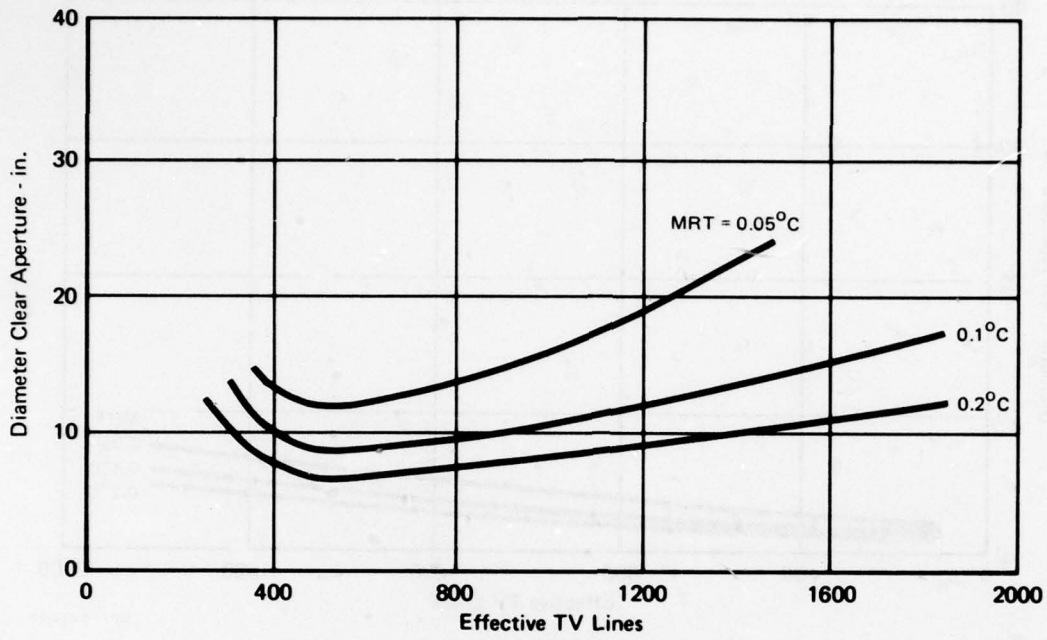
GP77-0292-14

FIGURE 15
2nd GENERATION DETECTOR LENS SIZE REQUIREMENTS
Wavelength: 8-14 μ Frequency: 0.7 c/mr
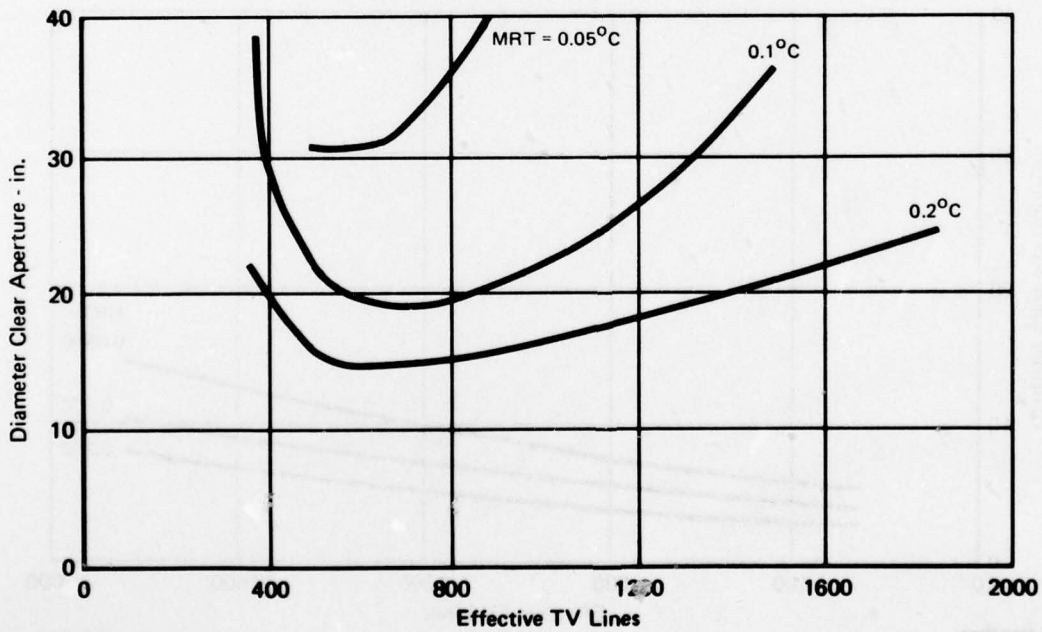
GP77-0292-13

FIGURE 16
2nd GENERATION DETECTOR LENS SIZE REQUIREMENTS
Wavelength: 8-14 μ Frequency: 1.0 c/mr
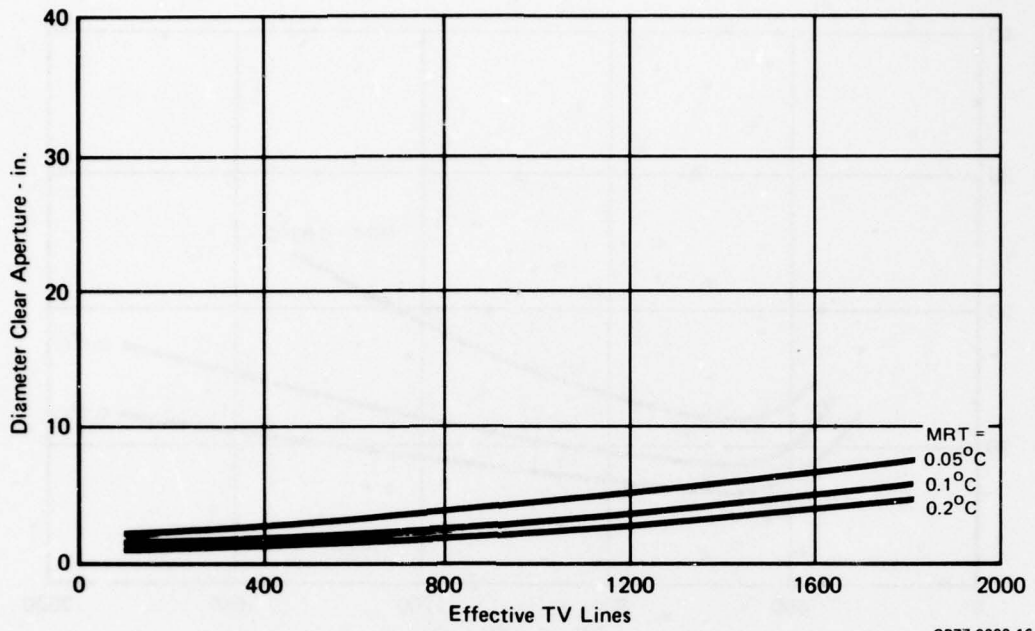
18
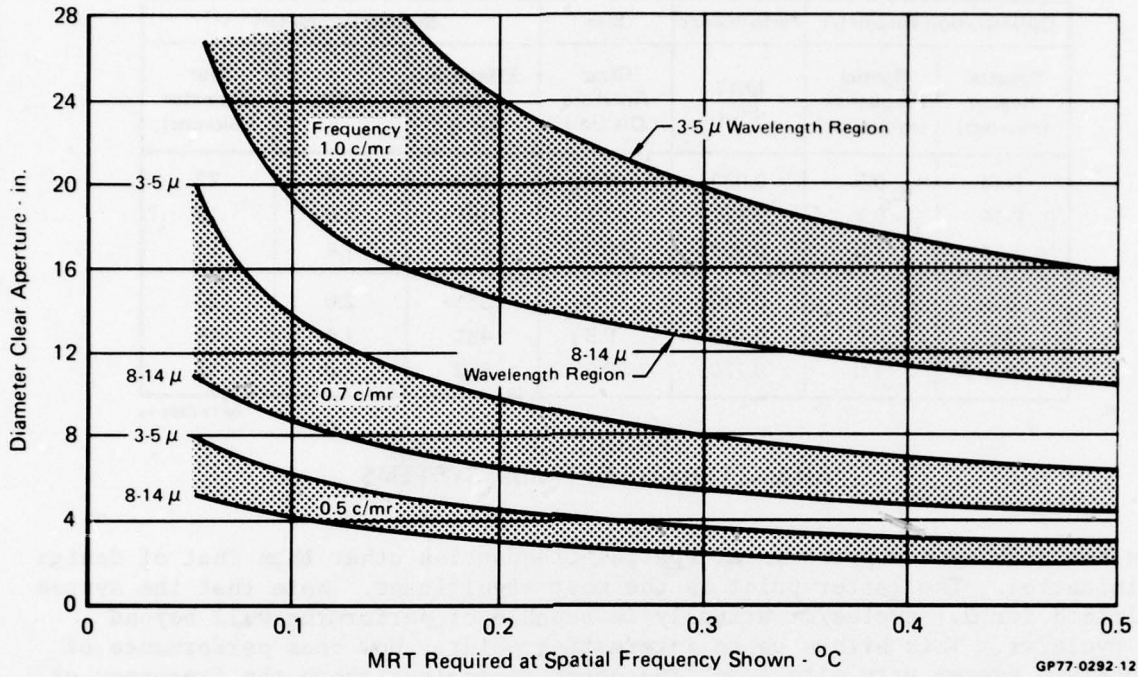
FIGURE 17
SIZE/PERFORMANCE PARAMETRICS 2ND GENERATION DETECTOR TECHNOLOGY
3-5 μ and 8-14 μ Spectral Regions
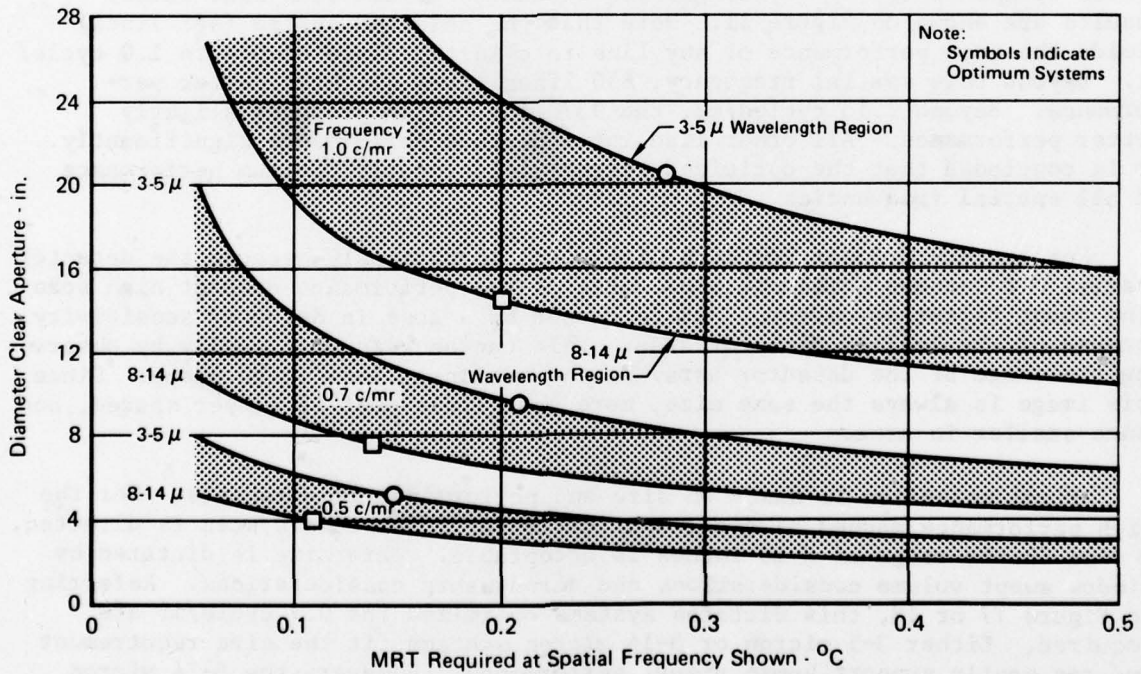
FIGURE 18
OPTIMUM SYSTEMS OF THE 2nd GENERATION DETECTOR TECHNOLOGY
3-5 μ and 8-14 μ Spectral Regions

Optimization Parameter		Performance	Size	System Parameters		
Spectral Region (microns)	Spatial Frequency (cycles/mr)	MRT (°C)	Clear Aperture Dia (in.)	Effective Scan Lines	F/No.	Blur Diameter (microns)
8-14	0.5	0.099	4.0	365	2.8	22
8-14	0.7	0.127	7.7	481	2.0	16
8-14	1.0	0.208	14.7	650	1.4	12
3-5	0.5	0.140	5.6	365	2.0	22
3-5	0.7	0.210	9.8	481	1.4	18
3-5	1.0	0.270	20.5	650	1.0	12

GP77-0292-18

FIGURE 19
PARAMETERS OF OPTIMUM SYSTEMS

show how each system performs at spatial frequencies other than that of design optimization. The latter point is the most significant. Note that the system optimized for 0.7 cycles/mr actually is capable of performing well beyond 1.0 cycle/mr. This brings up an interesting point. How does performance of an optimum system vary with scan line count in regions above the frequency of optimization? Scan line count could conceivably affect performance adversely since it was selected on the basis of a relatively low spatial frequency compared to the ultimate system performance. To study this, the 8-14 micron system optimized for 0.7 cycles/mr was evaluated at all scan line rates. Results are shown on Figure 21. Note that the selected system (481 lines) yields the best performance of any line rate in the range of 0.4 to 1.0 cycle/mr. Beyond this spatial frequency, 650 lines gives slightly better performance. Beyond 1.13 cycles/mr, the 937 line system produces slightly better performance. All other line rates degrade performance significantly. It is concluded that the optimized system yields nearly optimum performance at all spatial frequencies.

Performance drop at low scan line count is obviously because the detector spatial MTF becomes dominant. The cause of the performance drop at high scan line count is not so obvious. It is caused by a loss in detector sensitivity because of the smaller detector area. This can be seen most easily by observing the image of the detector array at the nonlinear lens image plane. Since this image is always the same size, more scan lines must be closer spaced, and hence smaller in area.

Final selection is based on size and performance requirements. For the high performance manned aircraft application at which this system is directed, a size in the range of 8-10 inches is acceptable. This size is dictated by window swept volume considerations and aerodynamic considerations. Referring to Figure 17 or 18, this dictates systems optimized for 0.7 cycle/mr are required. Either 3-5 micron or 8-14 micron systems fit the size requirement and can easily support human visual performance. However, the 8-14 micron system is significantly smaller. For these reasons, the 8-14 micron system is believed to be the best choice. Therefore, lens design for the second generation detector technology should be directed towards achieving an F/2.0 lens with a maximum blur sigma of 16 microns.
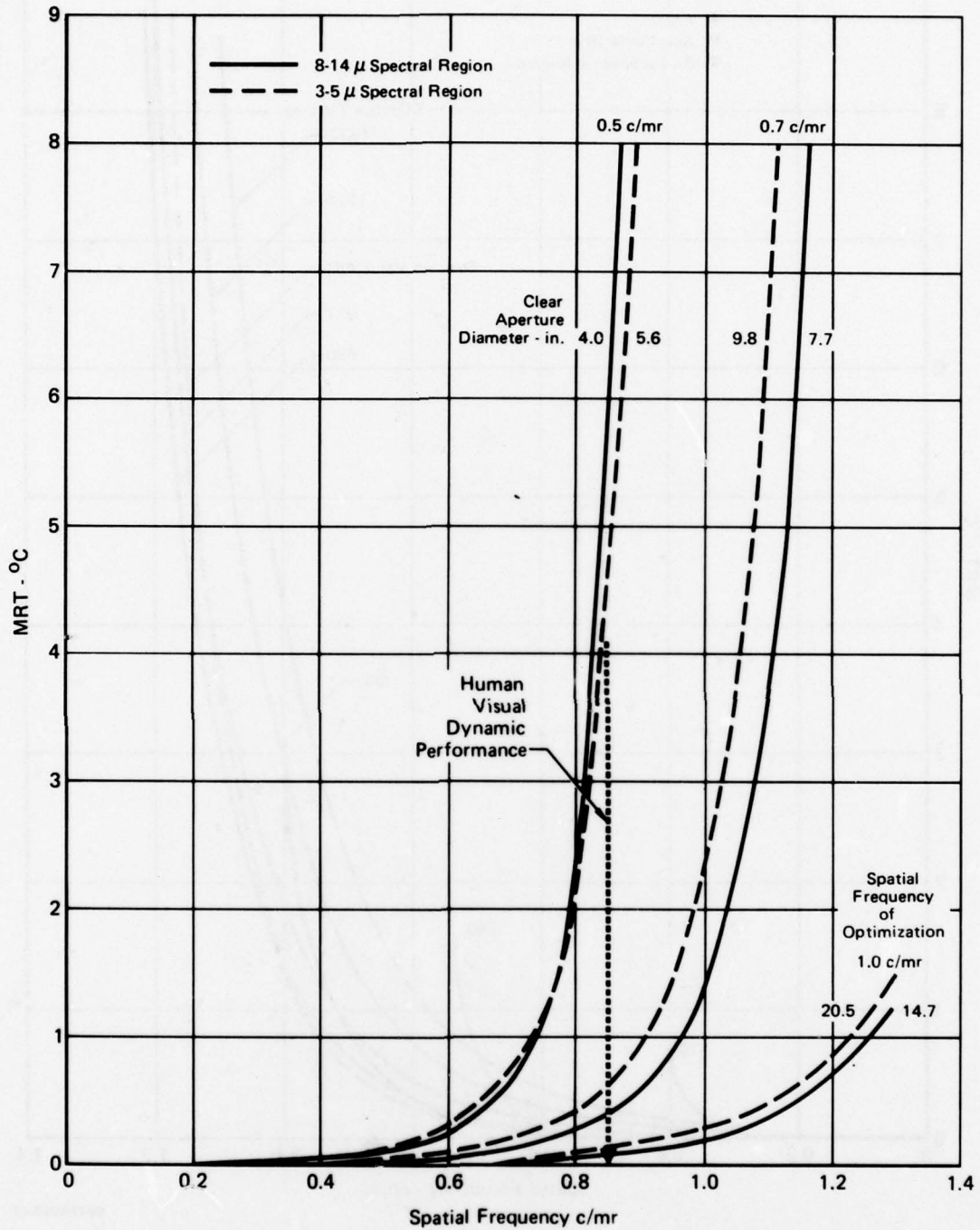
GP77-0292-19

FIGURE 20
MRT CURVES FOR OPTIMUM SYSTEMS
2nd Generation Detector Technology

21
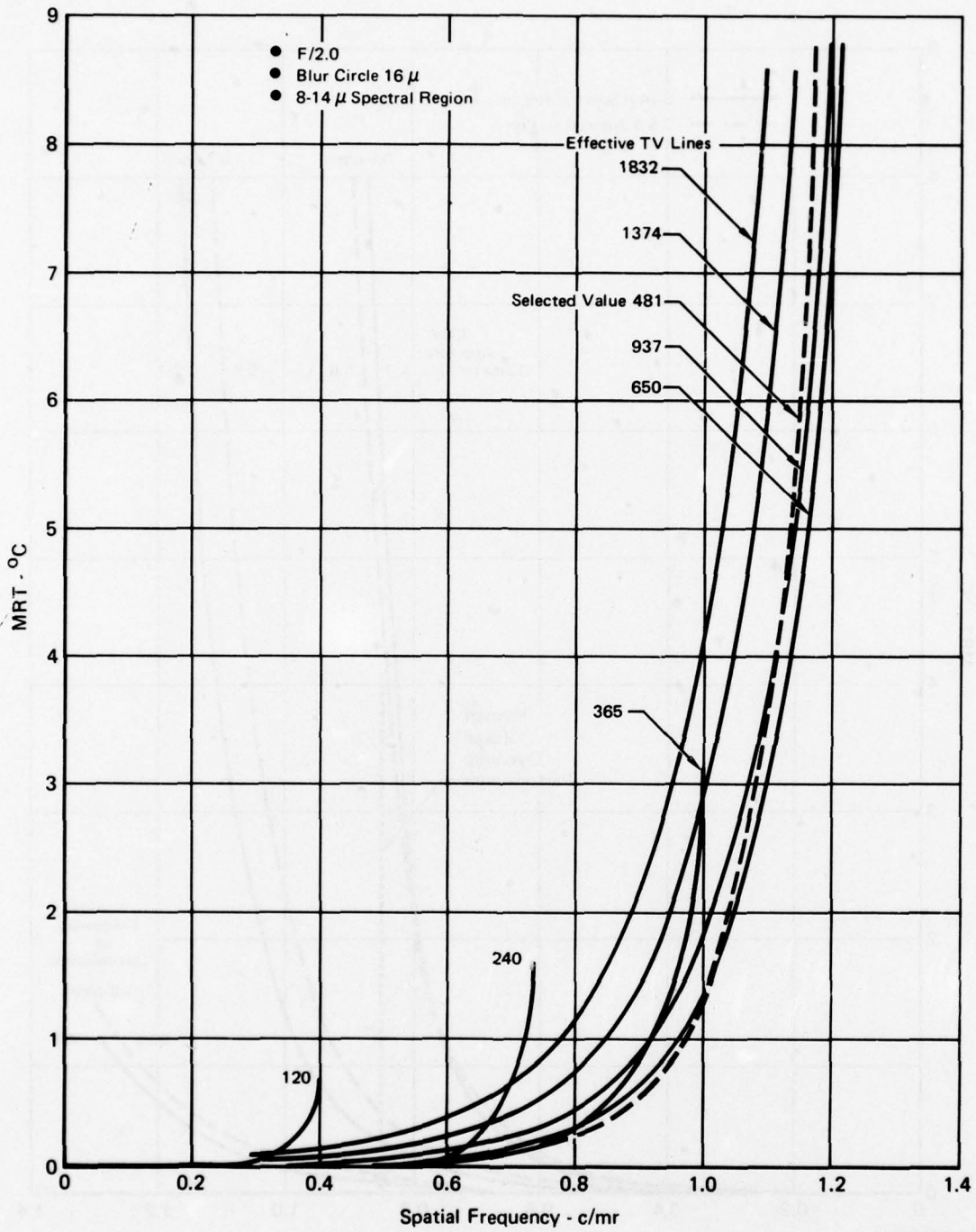
FIGURE 21
MRT FOR OPTIMUM 0.7 c/mr SYSTEM WITH 2ND GENERATION DETECTOR
AS A FUNCTION OF EFFECTIVE SCANNING LINE COUNT

22

RESULTS OF OPTIMIZATION ANALYSIS FOR CURRENT GENERATION SCANNER TECHNOLOGY

Current generation scanner technology analysis was performed under ONR contract[1]. Since the line rate is defined for the current generation scanners, selection proceeds immediately to Size vs MRT curves, similar to Figure 17 and which is presented on Figure 22. Note that sizes are similar to those of the second generation scanner systems but the performance (MRT) is not as good as the second generation systems. The F/number and blur of the optimum systems for 0.7 cycle/mr are approximately the same as they were in the second generation system. These are noted on Figure 22. Based on this observation, a non-linear lens having an F/2.0 and a blur of 16 microns maximum was also selected as the best lens for current generation scanners.

ANALYSIS CONCLUSIONS

The performance of all systems are compared on Figure 23. The advantages of the second generation detector technology is readily apparent from this data. The performance of the current generation scanners are comparable but the serial scanner has somewhat better performance.

As a final step, system MTF's are plotted for all four scanner systems. These are presented separately in Figures 24 through 27. Close observation of the MTF curves shows the relative balance achieved between all significant degrading phenomenon.

The analysis indicates that the F/2.0 lens with an optical blur sigma of 16 microns operating in the 8-14 micron spectral region is optimum. This lens can be used effectively with and is near optimum for either current or second generation detectors.

2.2 NARCISSUS ANALYSIS

Two types of narcissus analysis were conducted during this effort. The first was conducted to devise the most efficient method of relaying the lens image to the detector focal plane. In the second effort, actual narcissus imagery were located and its effect on system operation was predicted. Details of these analyses are presented below. Basic narcissus theory is presented in Appendix C.

RELAY NARCISSUS

Concern with the possible requirement for a field lens at the nonlinear lens focal plane necessitated an early parametric analysis of the optical relay with respect to narcissus effects. Narcissus is caused by the cold detector "seeing" itself as a result of reflections from relay optical surfaces. This relay is shown in general form in Figure 28. The function of this relay is to reimage the lens image of the real world onto the detector. This would be an easy optical task if it were not for the scanning mechanism which essentially translates the real world image across the detector. The scanning mechanism requires that all ray bundles cross at a common plane shown as the Effective Scanner stop of diameter D on Figure 28. A problem arises because the optical output of the nonlinear lens is not compatible with this requirement. The chief rays emerging from the image plane are not "well behaved" as they are in a conventional lens and therefore will not arrive at a common
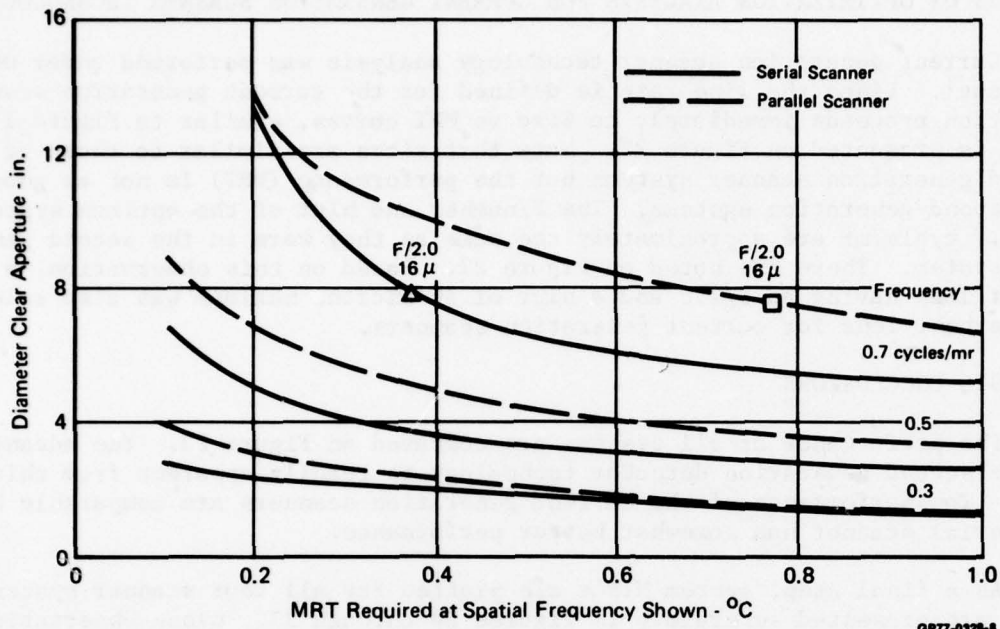
FIGURE 22
CURRENT GENERATION SCANNER SIZE/PERFORMANCE PARAMETRICS
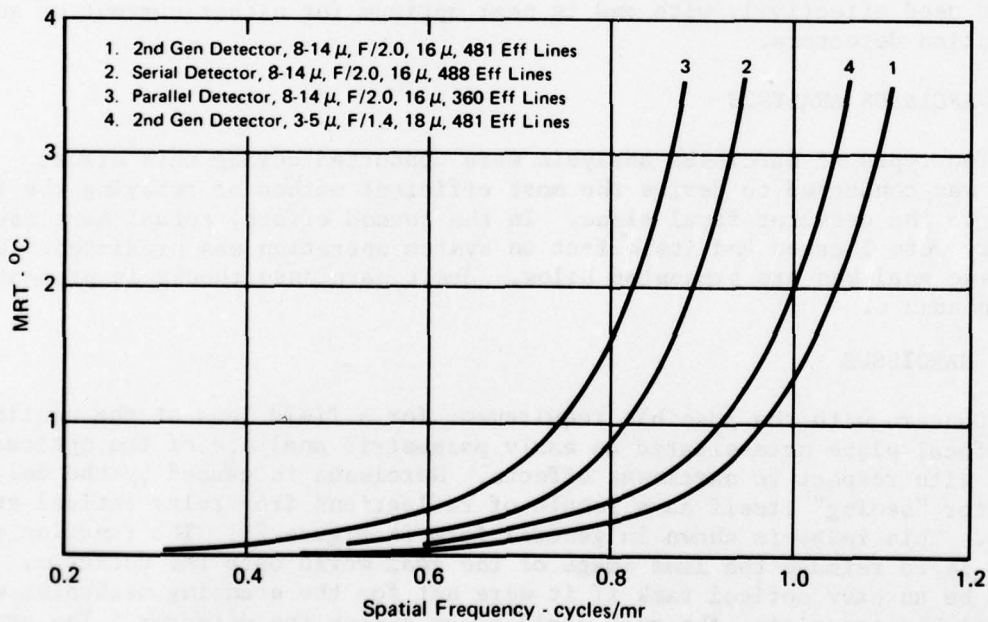
FIGURE 23
DETECTOR PERFORMANCE AS A FUNCTION OF RESOLUTION

FIGURE 24
SERIAL DETECTOR/NONLINEAR SYSTEM MTFs

F/2.0   Blur Circle 16μ   488 Line   8-14μ Spectral Region
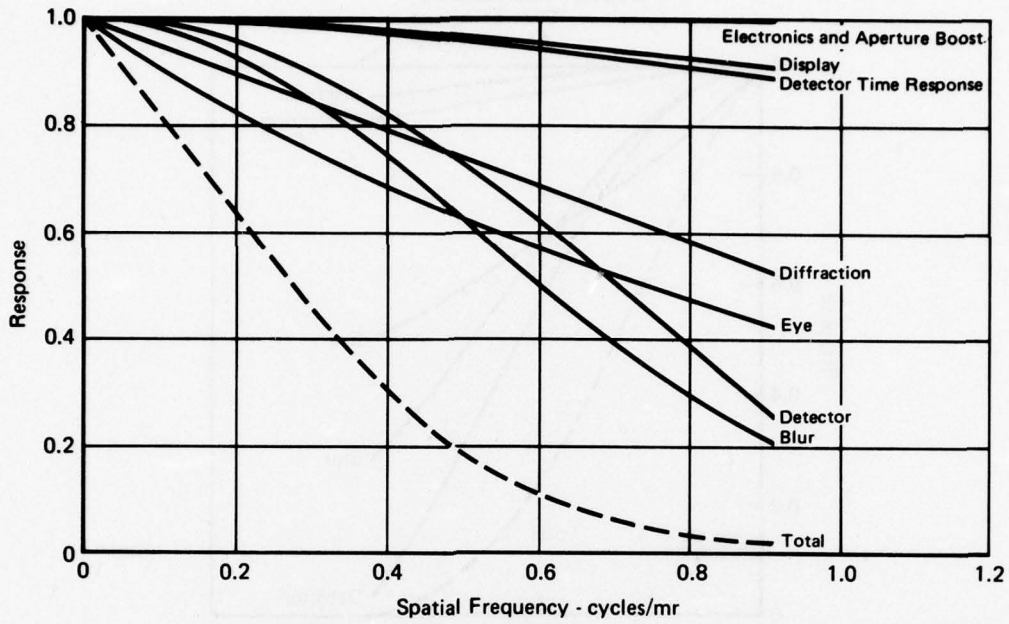
GP77-0328-5

FIGURE 25
PARALLEL DETECTOR/FOVEAL LENS SYSTEM MTF'S
F/2.0   Blur Circle 16μ   480 Lines   8-14 Spectral Region

GP77-0328-11

25
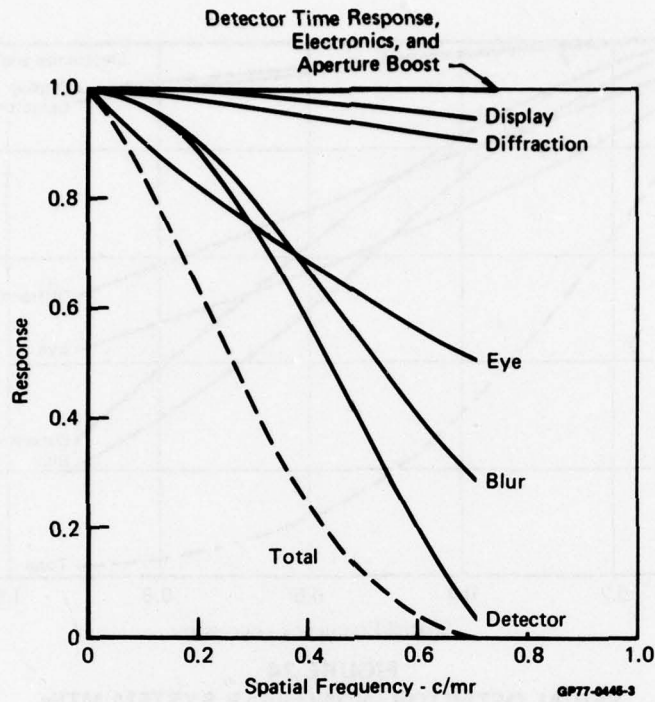
FIGURE 26
2nd GENERATION DETECTOR/NONLINEAR LENS SYSTEM MTF's
F/1.4 Blur Circle 18μ   481 Line   3-5μ Spectral Region
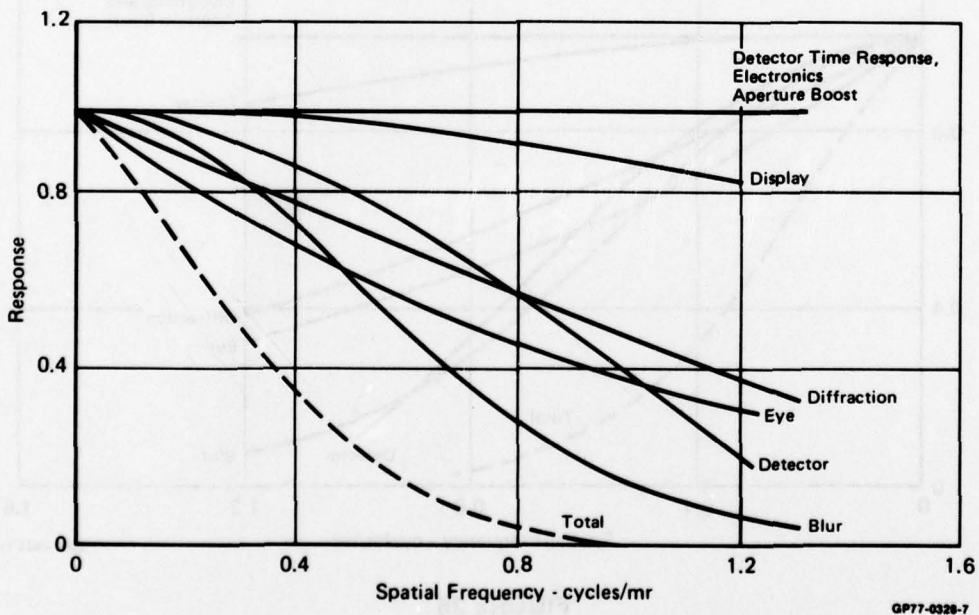
FIGURE 27
2nd GENERATION DETECTOR/NONLINEAR LENS SYSTEM MTF'S
F/2.0   Blur Circle 16μ   481 Line   8-14μ Spectral Region

26
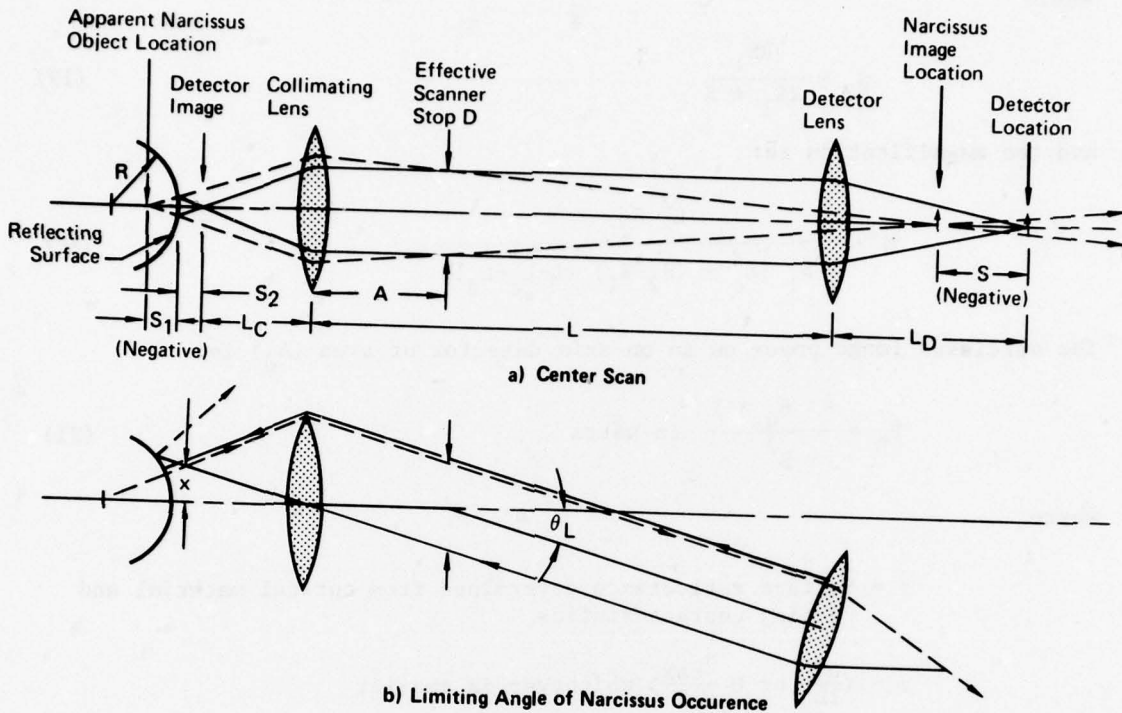
FIGURE 28
RVS RELAY AND NARCISSUS GEOMETRY

plane after collimation. This necessitates use of an aspheric field lens at the image plane. While field lenses create no special problem in visual systems, they can cause very serious "Narcissus" problems in the infrared spectrum. The geometry of narcissus is also shown in Figure 28.

It is easy to see how optical surfaces near any image plane generate the worst possible narcissus effects because they reflect and return the image back through the system with maximum efficiency. The field lens is in an ideal location to create this problem. For this reason, the narcissus theory developed in Appendix C was applied to this relay. For this study, a reflecting surface was theorized with curvature (R) and separation (S) from the nominal image location.

Narcissus theory requires that the location, size and strength of the narcissus image be known. This requires definition of the distance (S) from the narcissus image to the image plane, magnification of the image (M), and reflectance of the reflecting surface (τ), as shown in Figure 28. The first two can be determined from geometric optical theory. Using the definition of distances shown on Figure 28, the distance (S) and magnification (M) are:

$$S = \frac{L_D^2 \ (S_2 - S_1)}{L_c^2 + (S_2 - S_1) \ (L - L_c - L_d)} \qquad (18)$$

27

where

$$S_2 = \frac{RS_1}{2S_1 + R} \tag{19}$$

and the magnification is:

$$M = -\frac{L_c^2 S_2}{S_1 \left[L_c^2 + (S_2 - S_1) (L - L_c - L_d)\right]} \tag{20}$$

The narcissus image power on an on-axis detector of area (A_d) is:

$$P_D = \frac{4\tau A_d \, x \, y}{S^2} \quad \text{in watts} \tag{21}$$

where

τ = Surface reflectance determined from optical material and coating characteristics

$x = (\frac{DS}{2L_D}$ or $M \frac{a_{cax}}{2})$ whichever is smaller

$y = (\frac{DS}{2L_D}$ or $M \frac{a_{cay}}{2})$ whichever is smaller

$a_{cax, \, cay}$ = Effective cold assembly width, height

This is the worst case value which will occur at the center display scan position as shown in Figure 28. For other scan positions, narcissus returns are much more difficult to compute. However the maximum scan angle beyond which the narcissus return vanishes is relatively easy to predict. This occurs at the angle (θ_L) shown in Figure 28 where the marginal ray from the detector strikes the curved reflecting surface normally. At this scan angle only this ray returns. At greater scan angles the reflection does not pass through the stop and thus no narcissus exists. This maximum scan angle is

$$\theta_L = \text{arc tan} \left[\frac{D}{2 \left[\frac{L_c^2}{S_1 + R} + L_c - A \right]} \right] \tag{22}$$

or image position

$$x = \frac{L_c D}{2 \left[\frac{L_c^2}{S_1 + R} + L_c - A \right]} \tag{23}$$

If the image position (x) is divided by the format width, the portion of the display occupied by the narcissus image can be established.

The above theory was applied to the four scanners postulated in this study. Characteristics of these scanners and their required relay components are listed in Figure 29. Relay focal lengths were computed to match the detector plane to the lens focal plane as described previously in Section 2.1. The scanner input geometry was scaled to accommodate the F/2.0 lens output and to provide a full 1 inch by 1 inch scan format. The detector parameters of these four scanners that are required for narcisuus calculations are also listed in Figure 29. The data for the first three scanners, the Worst Case Serial, Probable Serial, and Parallel, is taken from ONR[3].

Scanner Type	Effective Cold Assembly Dimensions - cm		A_D - cm^2	NEP - watts	Lens Focal Length - in.		Separation (in.) (L)	A
	a_{cax}	a_{cay}			Collimating (L_C)	Detector (L_D)		
Worst Case Serial	0.3513	0.234	12.5×10^{-6}	8.05×10^{-11}	1.291	1	4	1
Probable Serial	0.116	0.0066	12.5×10^{-6}	8.05×10^{-11}	1.29	1	4	1
Parallel	0.0087	1.882	2.5×10^{-5}	2.57×10^{-11}	2.46	2.67	4	2
2nd Generation	0.038	1.504	12.5×10^{-6}	3.8×10^{-12}	1.29	1	4	1

GP77-0328-28

FIGURE 29
SCANNER PARAMETERS

The modified serial scanner includes a reflective detector surround to reduce narcissus. This narcissus reduction technique is also employed in the parallel scanner and is theorized for all second generation scanners.

The equations developed in previous paragraphs were applied to the relay designed for each scanner type to determine how the strength and the size of the narcissus return varies with respect to the image location (S_1) as location of the field lens surface and its radii of curvature (R_1) are changed. Separation (S_1) was varied $\pm$ 2 cm and four radii were used, ($\pm$ 1 cm, $\pm \infty$). The results are presented on Figures 30 to 37. Figures 30 and 31 show narcissus for the worst case serial scanner with positive and negative field lens radii. Note on Figure 30 that with a flat field lenses (infinite curvature $R_1 = \infty$), separation must be maintained greater than approximately $\pm$ 0.5 cm to make narcissus acceptable (below the NEP). If the field lens has positive radii, the negative separation must be increased. As shown on Figure 31, negative radii on the field lens reverses this situation.

29

a_cax = 0.3513 cm
a_cay = 0.234 cm

$R_1 = +1$ cm
$R_1 = +\infty$ cm

Negative Ratios

NEP = 8.05 (10⁻¹¹)

GP77-0269-2
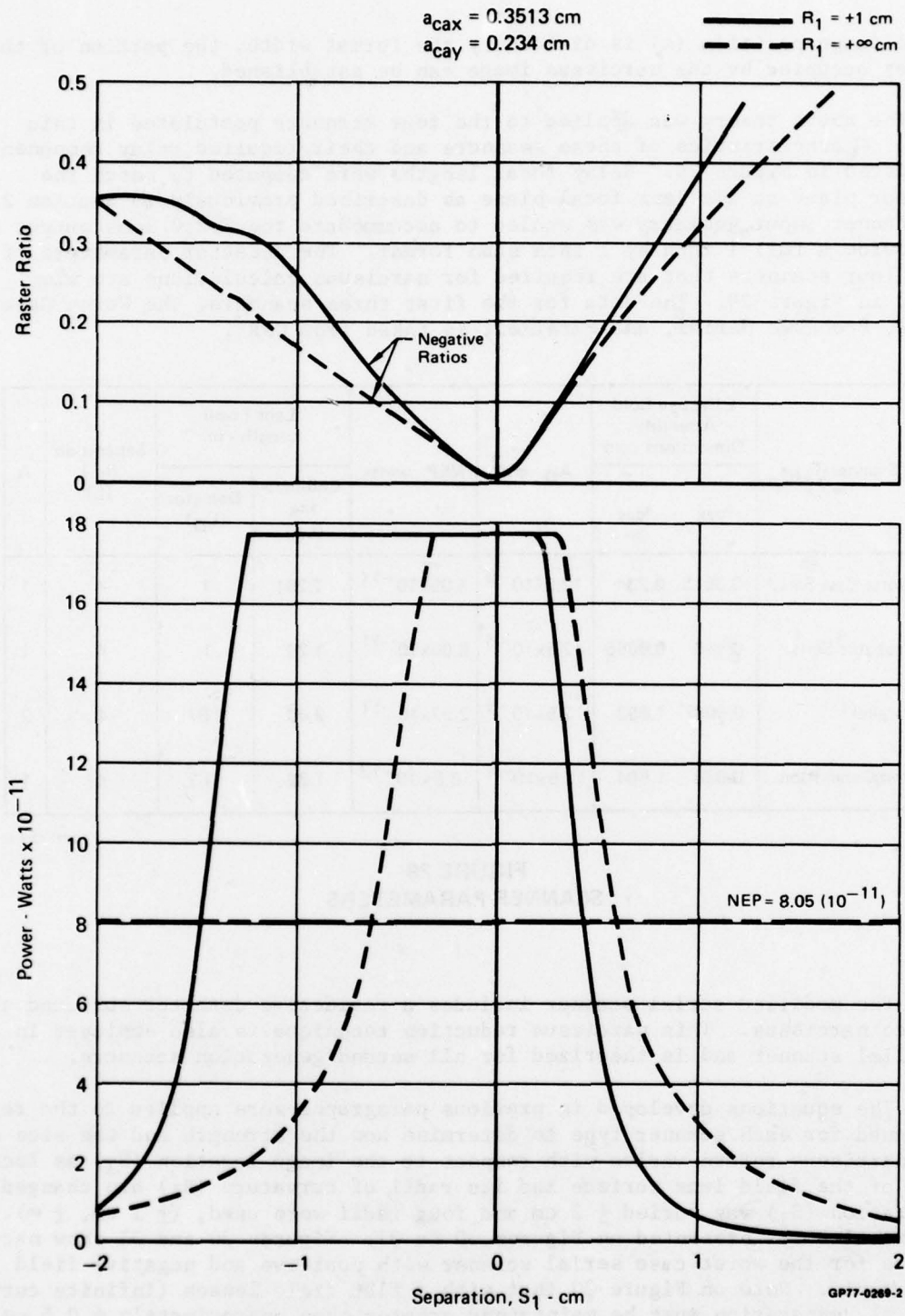
FIGURE 30
SERIAL SCAN ASSEMBLY
Positive Case

$a_{cax} = 0.3513$ cm ——— $R_1 = -1$ cm
$a_{cay} = 0.234$ cm - - - $R_1 = -\infty$ cm

Raster Ratio

Negative Ratio

Power - Watts x 10^{-11}

NEP = 8.05 (10^{-11})

Separation, S_1 - cm

GP77-0269-3
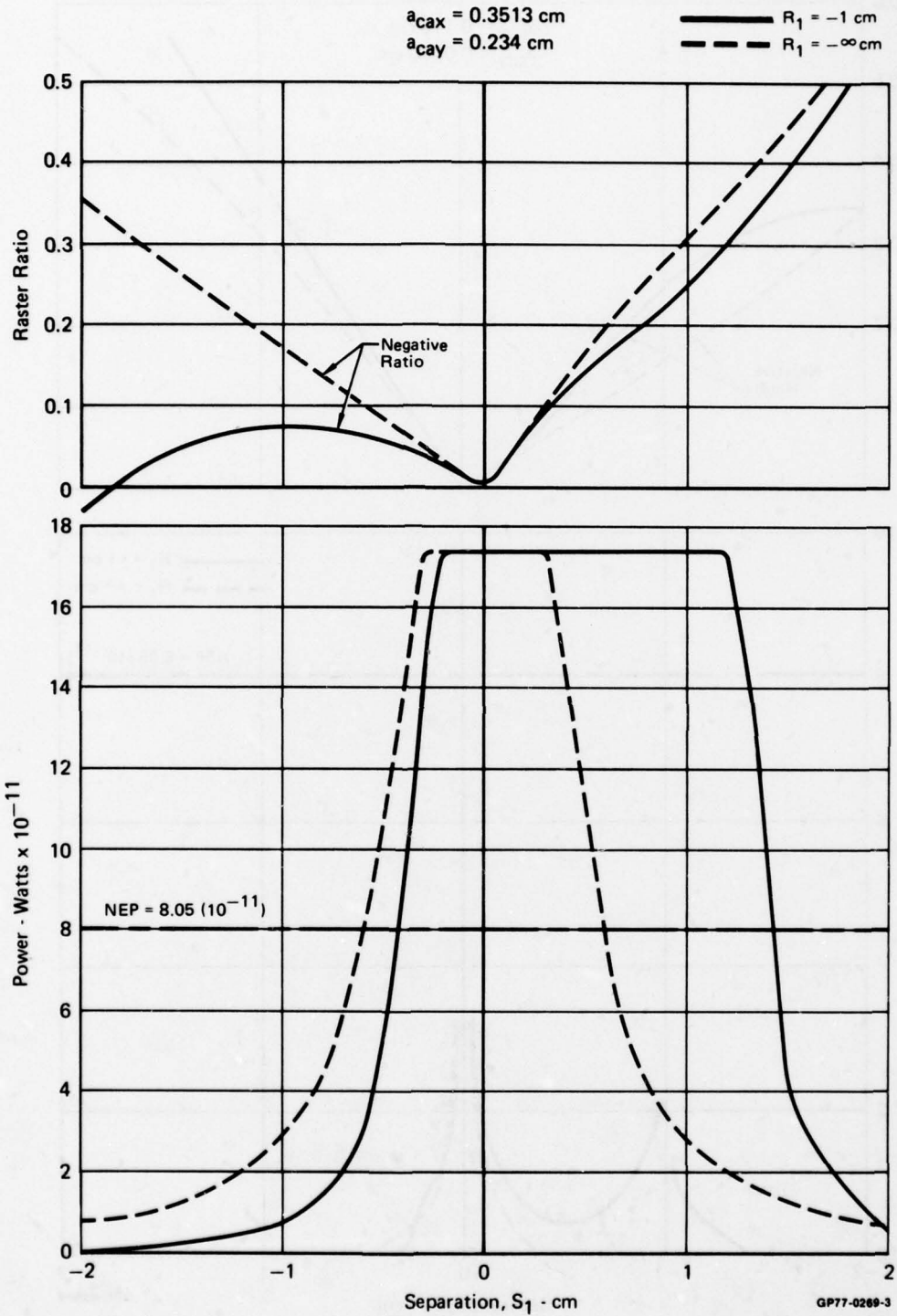
FIGURE 31
SERIAL SCAN ASSEMBLY
Negative Case

31
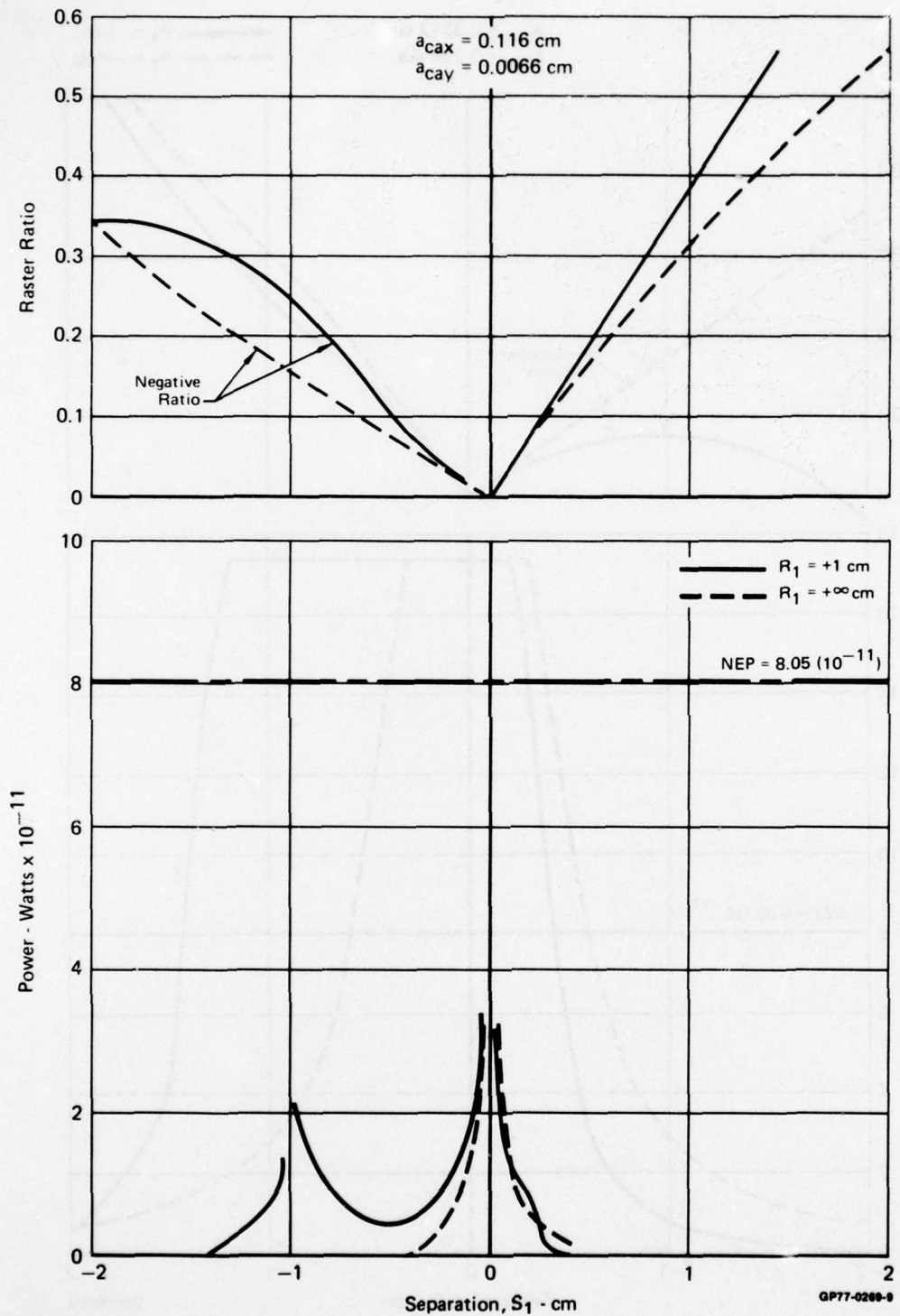
FIGURE 32
SERIAL SCAN ASSEMBLY WITH REFLECTIVE DETECTOR SURROUND NARCISSUS
AS A FUNCTION OF OBJECT POSITION (S1) AND REAR SURFACE CURVATURE (R)
Negative Case

32
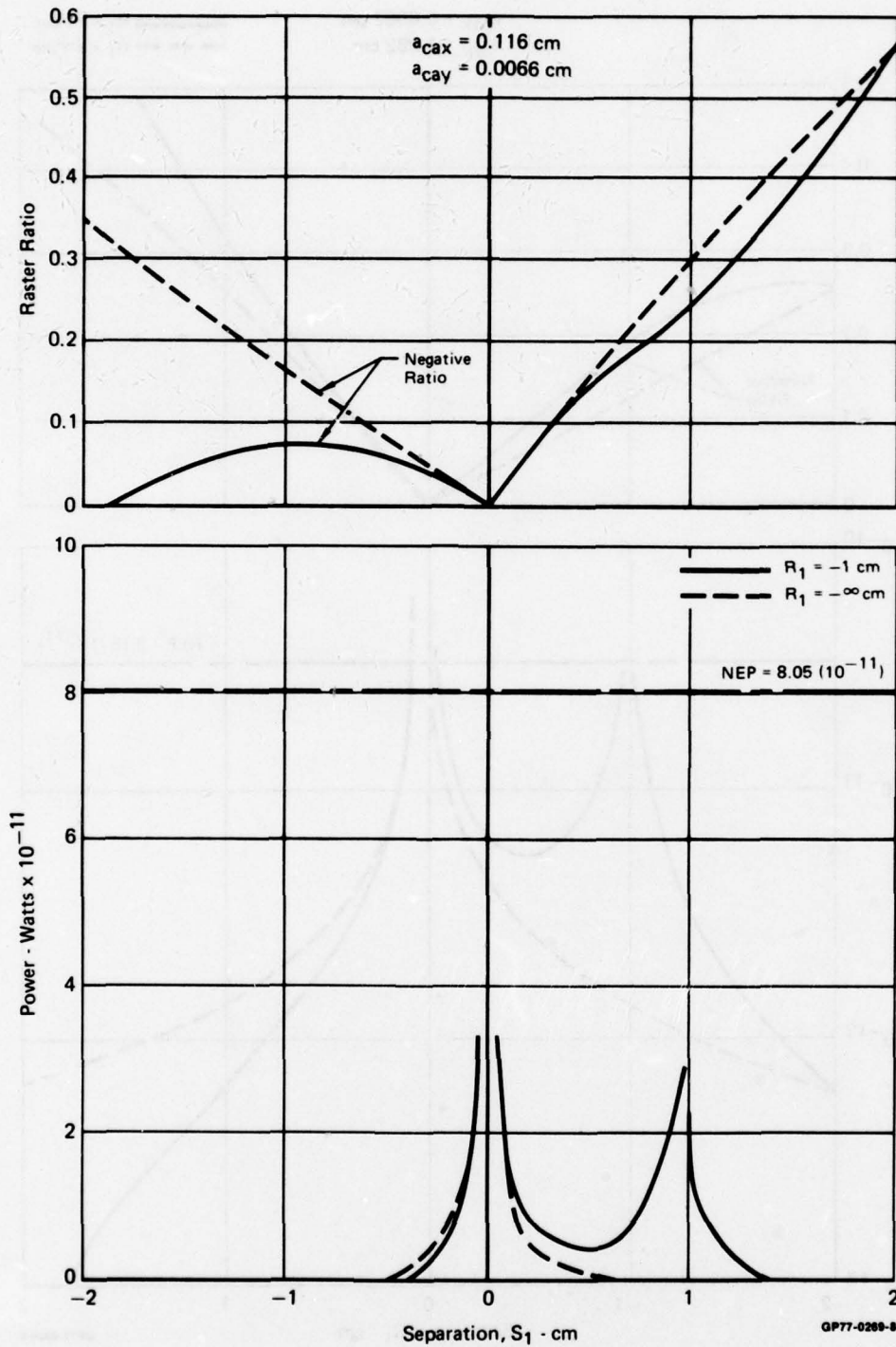
FIGURE 33
SERIAL SCAN ASSEMBLY WITH REFLECTIVE DETECTOR SURROUND NARCISSUS
AS A FUNCTION OF OBJECT POSITION (S1) AND REAR SURFACE CURVATURE (R)
Positive Case

33
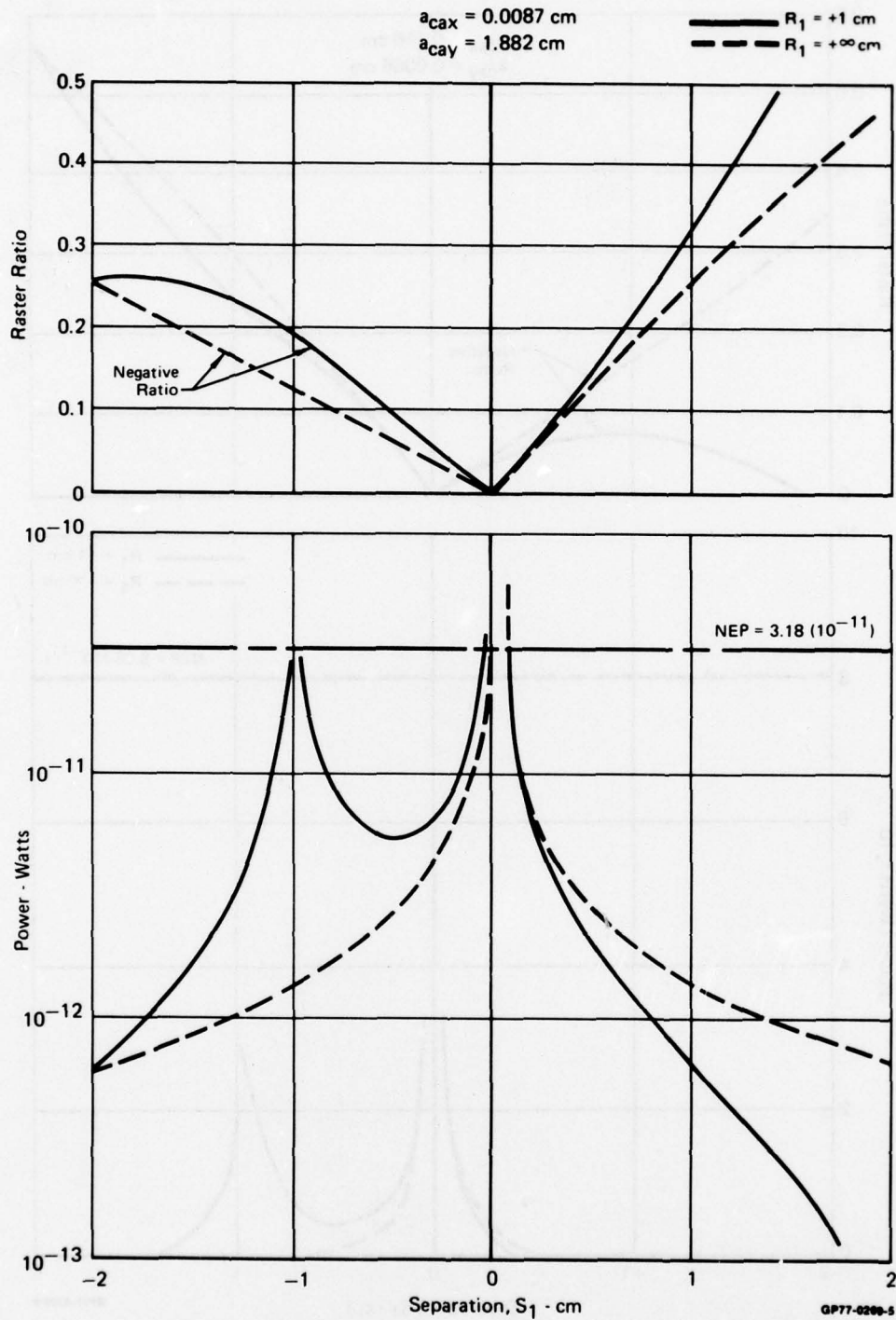
FIGURE 34
PARALLEL SCAN ASSEMBLY WITH REFLECTIVE DETECTOR SURROUND NARCISSUS
Posititive Case

34
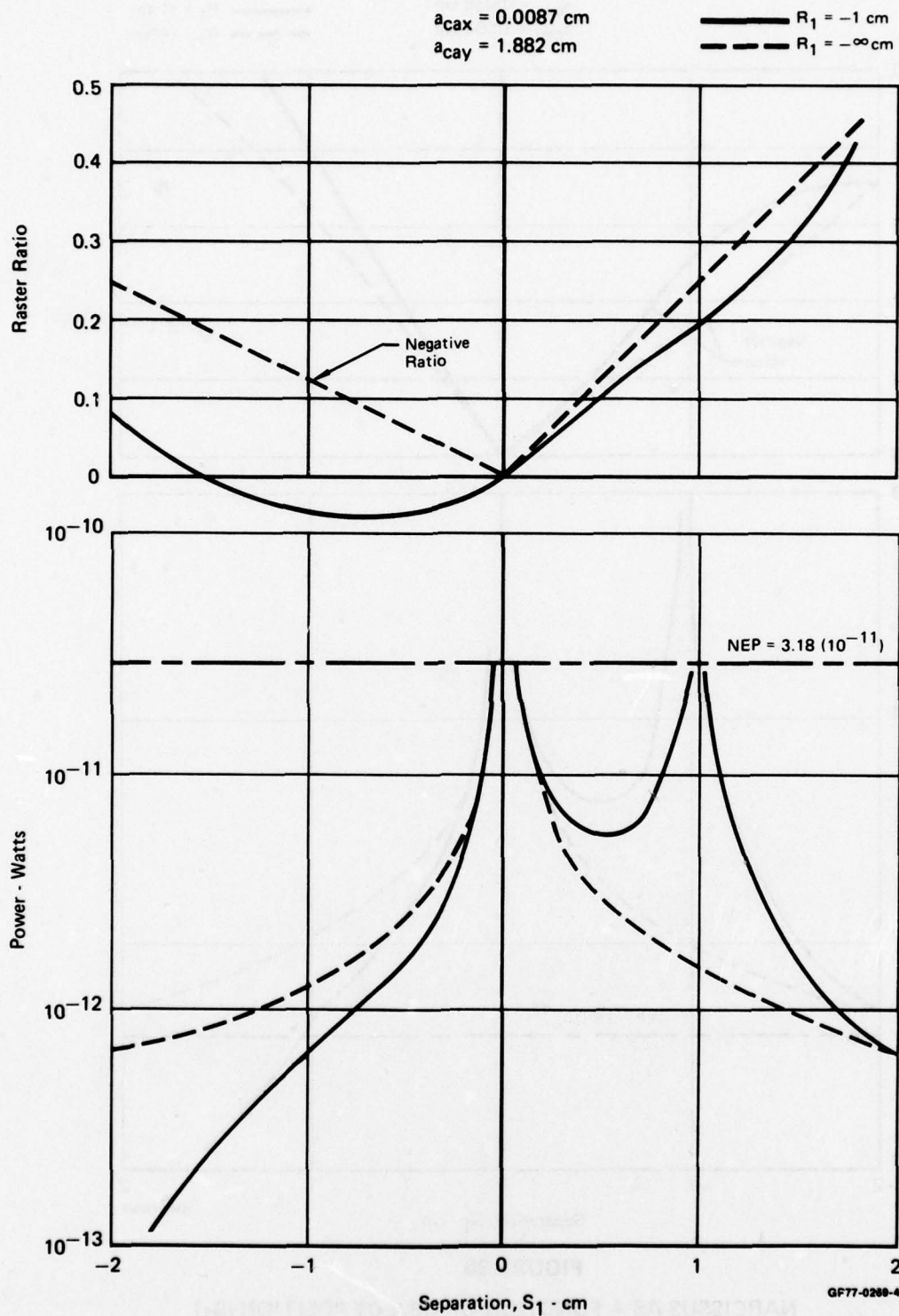
FIGURE 35
PARALLEL SCAN ASSEMBLY WITH REFLECTIVE DETECTOR SURROUND NARCISSUS
Negative Case

35

$a_{cax} = 0.038$ cm
$a_{cay} = 1.504$ cm

——— $R_1 = +1$ cm
- - - $R_1 = +\infty$ cm

Raster Ratio

0.5
0.4
0.3
0.2
0.1
0

Negative
Ratio

Power - Watts

10^{-9}
10^{-10}
10^{-11}
10^{-12}

NEP = $3.8 (10^{-12})$

-2   -1   0   1   2

Separation, S_1 - cm

GP77-0269-7
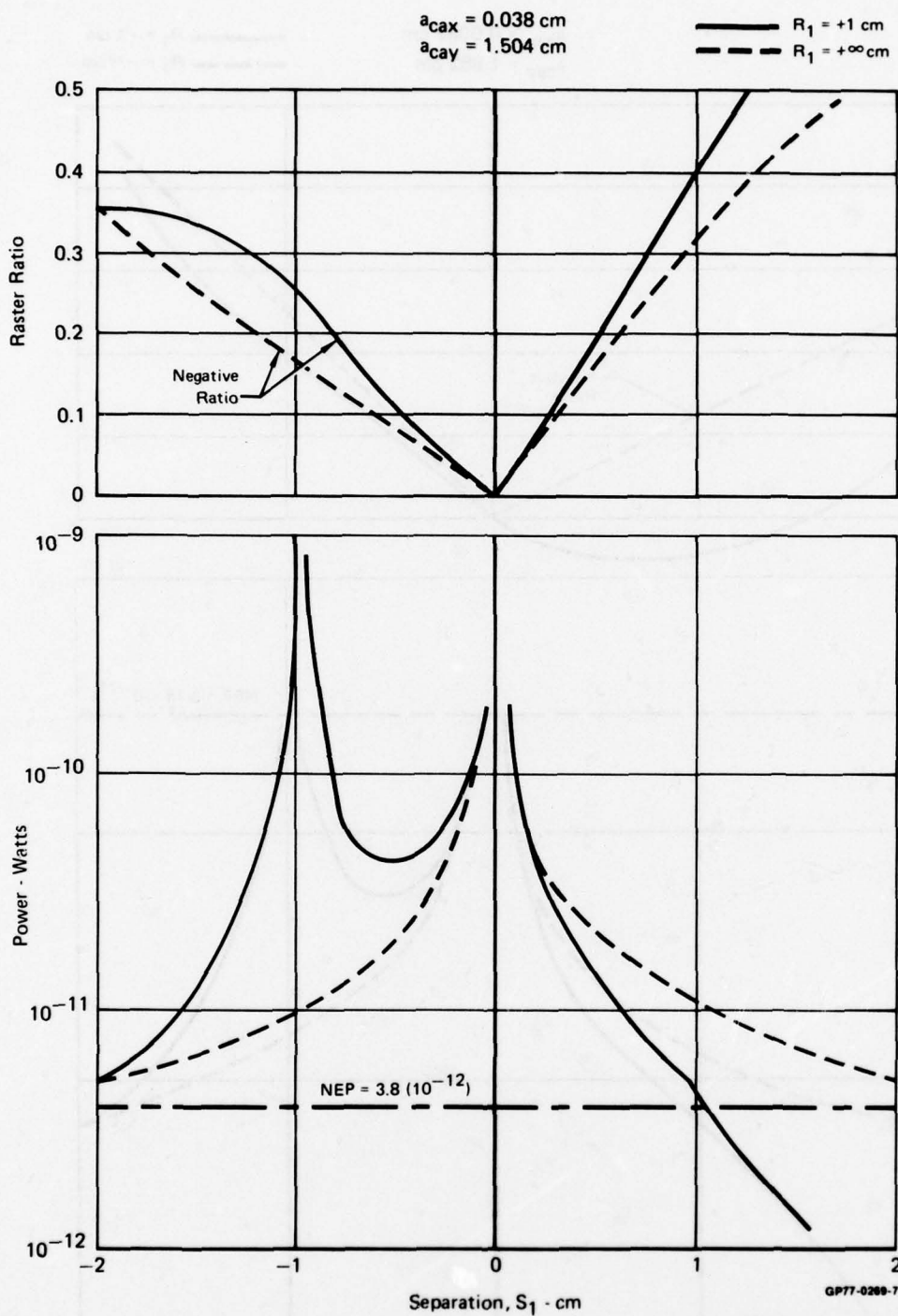
FIGURE 36

NARCISSUS AS A FUNCTION OF OBJECT POSITION (S_1)
REAR SURFACE CURVATURE (R)
2nd Generator Detector Assembly
500 x 10 Detectors   Positive Case

36
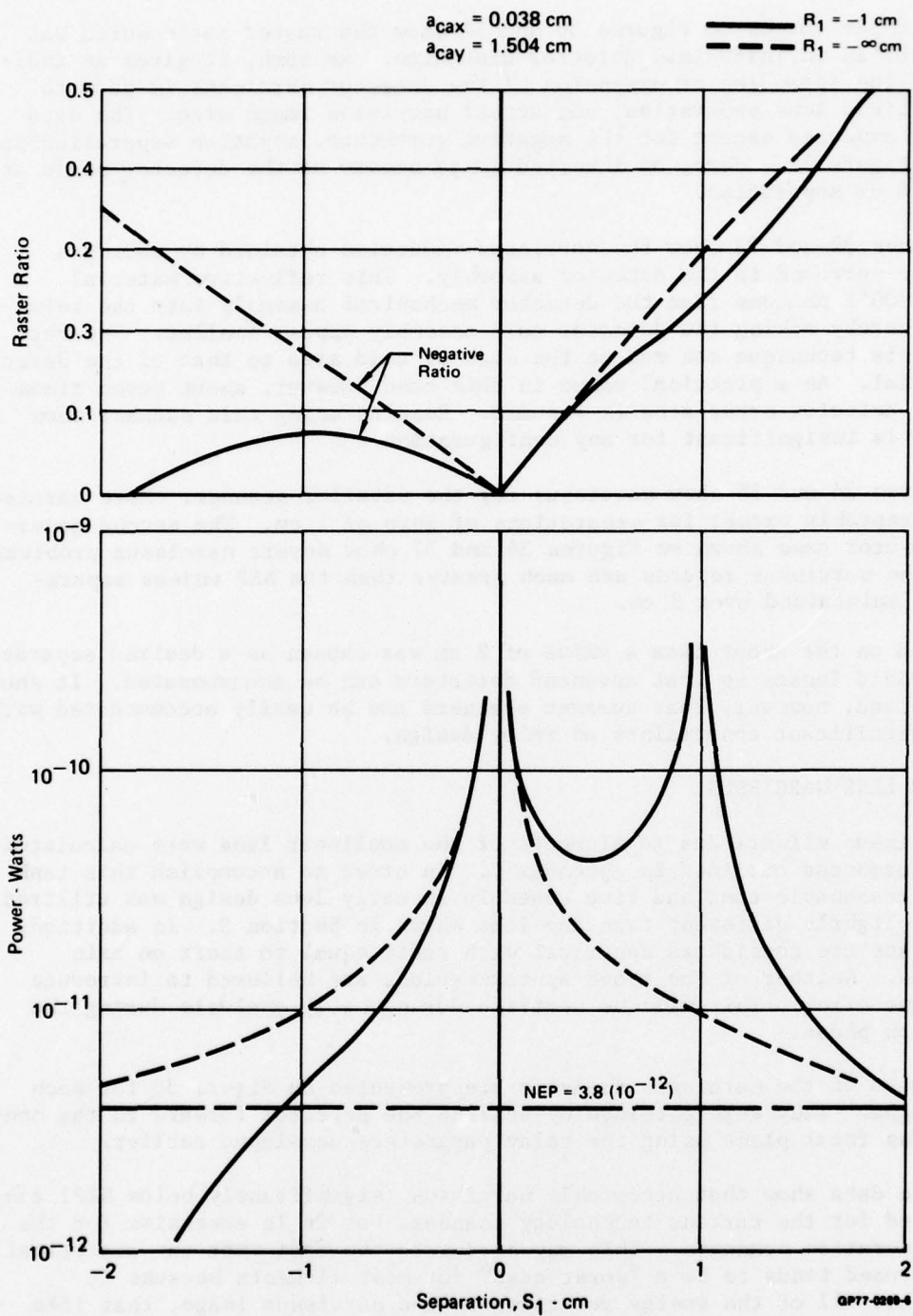
FIGURE 37

NARCISSUS AS A FUNCTION OF OBJECT POSITION (S₁)
AND REAR SURFACE CURVATURE (R)
2nd Generator Detector Assembly
500 x 10 Detectors   Negative Case

37

The upper curves on Figures 30 and 31 show the raster ratio which was derived for an infinitesimal detector dimension. As such, it gives an indication of the spreading or expansion of the detector narcissus image with detector field lens separation, not actual narcissus image size. The data shown was expected except for the negative curvature, negative separation case shown in Figure 31. Here, an inverted image occurs at the detector plane at about -1.8 cm separation.

Figures 32 and 33 show the narcissus reduction obtained by adding a reflective surround to the detector assembly. This reflective material reflects 300°K photons from the detector mechanical assembly into the relay optics, thereby making the detector cold assembly appear smaller. Theoretically, this technique can reduce the size of cold area to that of the detector material. As a practical value in this case however, about seven times the total detector array area is assumed. Results using this scanner show narcissus is insignificant for any configuration.

Figures 34 and 35 show narcissus for the parallel scanner. Here narcissus is acceptable except for separations of zero of 1 cm. The second generation detector case shown on Figures 36 and 37 show severe narcissus problems because the narcissus returns are much greater than the NEP unless separations are maintained over 2 cm.

Based on the above data a value of 2 cm was chosen as a desired separation for any field lenses so that advanced detectors can be accommodated. It should be emphasized, however, that current scanners can be easily accommodated without any significant constraints on relay design.

NONLINEAR LENS NARCISSUS

Narcissus effects due to elements of the nonlinear lens were calculated by the procedures outlined in Appendix C. In order to accomplish this task within a reasonable cost and time schedule an early lens design was utilized which is slightly different than the lens shown in Section 3. In addition, all elements are considered spherical with radii equal to their on axis curvatures. Neither of the above approximations are believed to introduce significant error. This will be verified during early analysis during the fabrication phase.

Results of the narcissus analysis are presented on Figure 38 for each scanner type. They were obtained by scaling the detector forward to the nonlinear lens focal plane using the relay parameters developed earlier.

These data show that acceptable narcissus (significantly below NEP) can be obtained for the current technology scanners but it is excessive for the second generation scanners. This may be due to the fact that the analytical technique used tends to be a "worst case" for most elements because it assumes that all of the energy returning to the narcissus image, that lies within the on axis detector ray line, will illuminate this detector (Figure C-5 of Appendix C). For elements well forward of the image plane this is quite often not the case. Usually much of the energy from off-axis detector cold assembly points that should return and strike the detector is lost on the return path. This is illustrated by ray trace data that was very laboriously obtained on narcissus from the extreme front surface. This narcissus data is listed on the bottom of Figure 33 and can be directly compared to the last

38

Surface	S_1 cm	Mag	Worst Case Serial	Modified Serial	2nd Generation	Parallel
1	3.889	−0.4408	1.503×10^{-11} (0.186)	1.4×10^{-14} (0.000174)	1.045×10^{-12} (0.275)	1.545×10^{-13} (0.00594)
2	0.3109	0.8996	2.135×10^{-10} (2.652)	9.126×10^{-12} (0.1134)	6.063×10^{-11} (15.9)	1.005×10^{-11} (0.3865)
3	0.652	0.8829	1.747×10^{-10} (2.17)	1.999×10^{-12} (0.0248)	2.837×10^{-11} (7.47)	4.702×10^{-12} (0.181)
4	0.8250	1.038	1.623×10^{-10} (2.016)	1.725×10^{-12} (0.02143)	2.636×10^{-11} (6.94)	4.368×10^{-12} (0.168)
5	0.8397	1.028	1.580×10^{-10} (1.96)	1.634×10^{-12} (0.0203)	2.565×10^{-11} (6.75)	4.251×10^{-12} (0.163)
6	6.751	1.743	7.801×10^{-12} (0.097)	7.26×10^{-14} (0.0009)	5.41×10^{-12} (1.42)	8.014×10^{-13} (0.031)
7	0.4983	0.4536	9.697×10^{-11} (1.205)	9.03×10^{-13} (0.01122)	1.907×10^{-11} (5.02)	3.161×10^{-12} (0.1216)
8	0.7752	0.1652	5.315×10^{-12} (0.06596)	4.95×10^{-14} (0.00061)	3.695×10^{-12} (0.972)	5.460×10^{-13} (0.021)
8 Detailed Ray Trace	0.7752	0.1652	3.879×10^{-13} (0.00482)	3.305×10^{-14} (0.00041)	1.903×10^{-13} (0.05)	3.153×10^{-14} (0.001213)
NEP			8.05×10^{-11}	8.05×10^{-11}	3.8×10^{-12}	2.6×10^{-11}

Note:
Figure in parenthesis is ratio of narcissis power divided by NEP.

GP77-0328-27

FIGURE 38
NARCISSUS FROM NONLINEAR LENS SURFACES

value of the approximate data. In general, narcissus is lower by more than
an order of magnitude when computed by this more exact technique. An excep-
tion is the modified serial scanner where the source is so small that very
little energy is lost on the return path. For elements located close to the
focal plane, the probability of losing energy becomes much less and the
approximate method for computing narcissus (Appendix C) should become more
accurate.

NARCISSUS CONCLUSIONS

Narcissus, while being somewhat less than that indicated on Figure 38,
will be unacceptable for the next generation FLIR unless dynamic compensation
is incorporated. This could be accomplished on a linear scan system
by storing an entire scan frame and subtracting out the narcissus bias.
Another technique would employ a rotating scan array to take advantage of
the rotational symmetry inherent in the narcissus returns of the nonlinear
lens. A full two-dimensional non-scanned array also would inherently elimi-
nate narcissus.

Section 3

LENS DESIGN AND OPTIMIZATION

The lens design phase proceeded along lines shown in Figure 39. The effort started with a materials survey to find the best material for construction of the infrared nonlinear lens. Initially, materials suitable for operation in either the 3-5 micron or 8-14 micron regions were considered. Conclusions were to use silicon for the 3-5 micron spectrum and germanium for the 8-14 micron spectrum for the severe aspherics. The remaining elements could be made of other materials based on disperison requirements. The primary reason for the aspheric element selection was advice from the lens fabricator, Frank Cooke. Both materials can be worked as easily as glass and present no problems of fabrication. In addition these materials can be obtained with very good homogeneity where all other materials are questionable in this area. Considering the thickness of the large aspheric elements, homogeneity is of upmost importance. Another reason for selecting silicon and germanium, are their low dispersions in their respective operating regions. The dispersion is nearly an order of magnitude smaller than that of any other applicable material. Low dispersion greatly simplifies optical design, especially in an unconventional design such as this one. Finally, both materials have good stable mechanical and thermal characteristics. The only disadvantage of these materials is their high index of refraction but this does not impose any restriction on design. It does, however, require sophisticated optical coatings to maintain high transmission. The required coating technology exists and does not outweigh advantages of employing the high index materials.

As the analysis progressed the 8-14 micron spectral region was selected as optimum and therefore the material used is limited to germanium. It was later shown that because of its low dispersion the entire lens could be made of germanium.

The next step in lens design was to initialize the existing lens computer program with parameters of the IR lens and establish a first order design for a single wavelength. An index of 4.003 was used with an 8 inch clear aperture diameter and the original nonlinear lens distortion function. The initial design was established for an 11 micron wavelength F/2.0 aperture.

The target in the next design iteration, was a lens with an optical blur of no greater than 16 microns when imaging over the entire 8-14 micron spectral region. After an acceptable design was achieved, modifications were attempted to produce a well behaved optical output from the image plane, to facilitate optical relaying to the scanner and detector. In general, this consisted of establishing a fixed exit pupil for the F/2.0 ray cone output by using aspheric field lens surfaces. The design was iterated until a fixed pupil was achieved.

As the narcissus analysis progressed in the Analytical Phase of the effort, it became apparent that narcissus placed severe constraints on location and curvatures of field lens surfaces. Based on this data, it was necessary to reiterate the design while forcing the field lens surfaces away from the lens

40
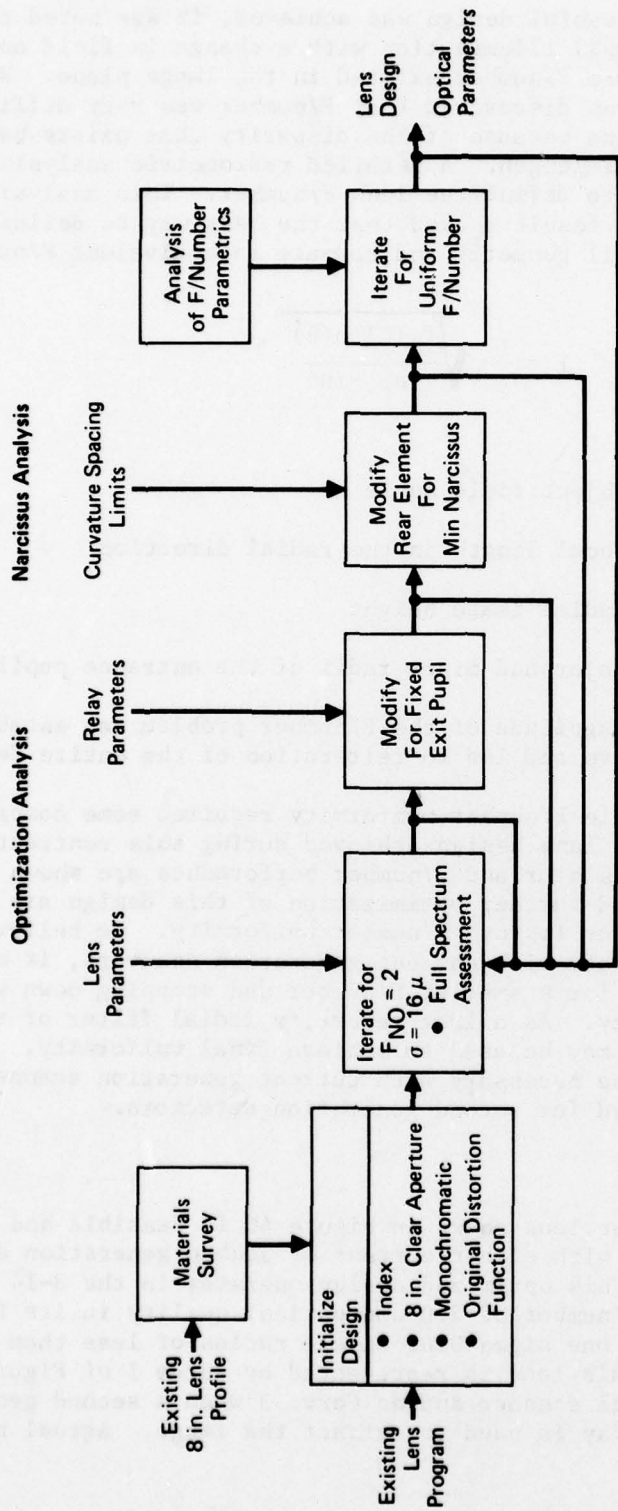
FIGURE 39

LENS DESIGN AND OPTIMIZATION

GP77-0328-2

Existing 8 in. Lens Profile

Existing Lens Program

Materials Survey

Initialize Design
• Index
• 8 in. Clear Aperture
• Monochromatic
• Original Distortion Function

Iterate for $F_{NO} = 2$
$\sigma = 16\mu$
• Full Spectrum Assessment

Lens Parameters

Modify For Fixed Exit Pupil

Optimization Analysis
Relay Parameters

Modify Rear Element For Min Narcissus

Narcissus Analysis
Curvature Spacing Limits

Iterate For Uniform F/Number

Analysis of F/Number Parametrics

Lens Design
Optical Parameters

image plane. After a successful design was achieved, it was noted that there was a variation in exit pupil illumination with a change in field angle. This indicated that a non-uniform F/number existed in the image plane. When this problem was examined, it was discovered that F/number was very difficult to define on the nonlinear lens because of the disparity that exists between radial and tangential focal length. A detailed radiometric analysis was required to determine how to define the lens F/number. This analysis is presented in Appendix D. The result showed that the best way to define F/number was to define entrance pupil geometry and compute an equivalent F/number by:

$$F = \frac{1}{2} \sqrt{\frac{f_r(\theta) \ h(\theta)}{ab \ \sin\theta}} \qquad (24)$$

where

θ = Object field angle

$f_r(\theta)$ = Focal length in the radial direction

$h(\theta)$ = Radial image height

a and b = Major and minor radii of the entrance pupil ellipse.

Using this equation, the magnitude of the F/number problem was established. It was found to be excessive and led to reiteration of the entire design.

Achieving an acceptable F/number uniformity required some compromise in relay narcissus. The best lens design achieved during this contracted effort is shown in Figure 40. Its blur and F/number performance are shown on Figure 41. Reiteration and further optimization of this design are continuing in an attempt to further improve F/number uniformity. We believe it can be made acceptable to operate with current generation scanners, if not by design, then by designing for a smaller F/number and stopping down within the relay to achieve uniformity. As a last resort, a radial filter or variable thickness element coating may be used to achieve final uniformity. However, we do not feel this will be necessary with current generation scanners but will definitely be required for second generation detectors.

CONCLUSIONS

The infrared nonlinear lens shown in Figure 40 is feasible and can fully support the VARVS concept with either current or second generation detector and scanner technology. This optimized design operates in the 8-14 micron spectral region, has an F/number of 2.0 and optical quality in its focal plane is represented by a one sigma blur circle radius of less than 16 microns. System performance with this lens is represented by Curve 1 of Figure 42 with a current generation serial scanner and as Curve 3 when a second generation monolithic focal plane array is used to extract the image. Actual performance
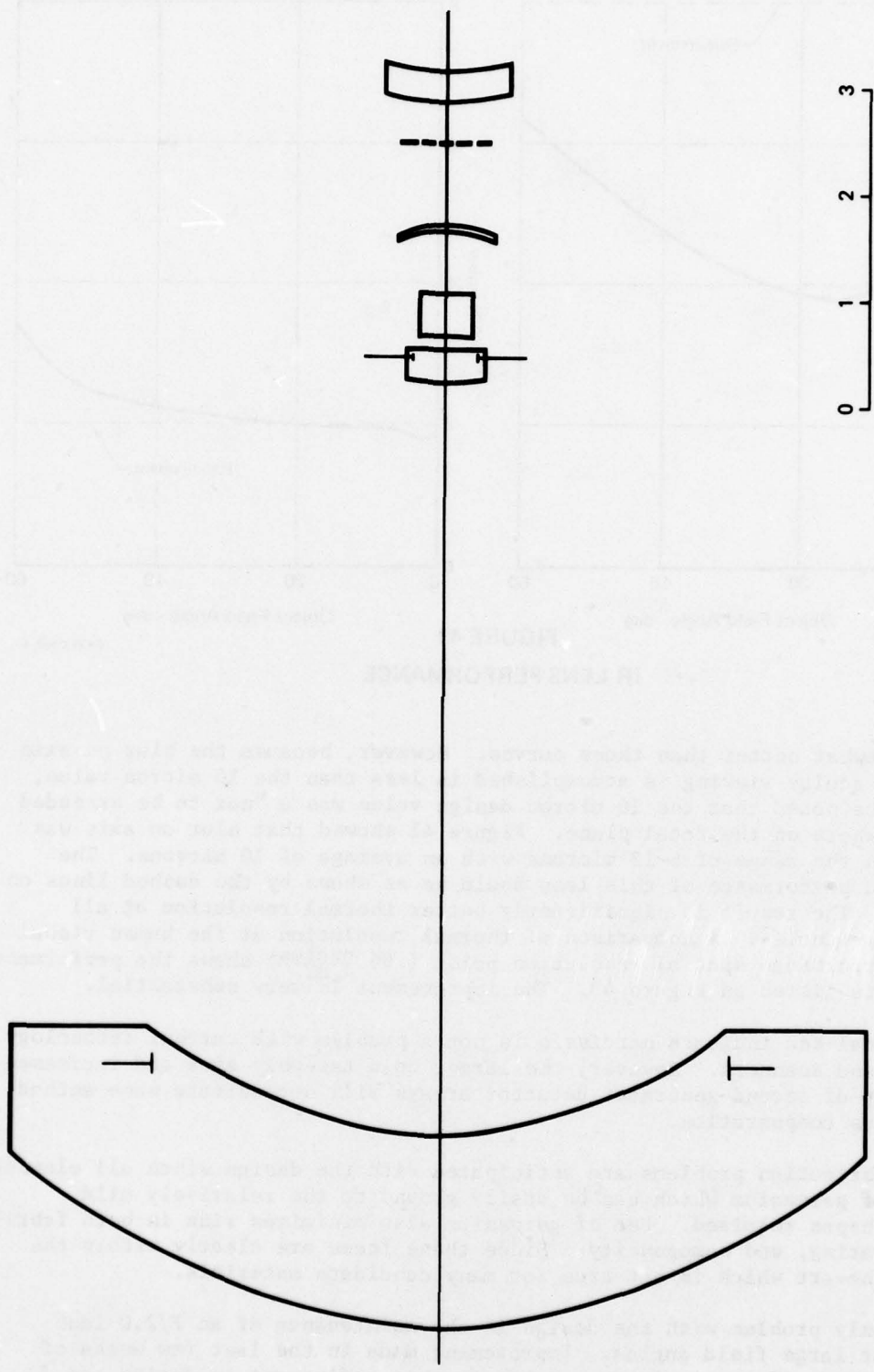
**FIGURE 40
INFRARED NONLINEAR LENS**

GP77-0348-7

Scale in inches

43
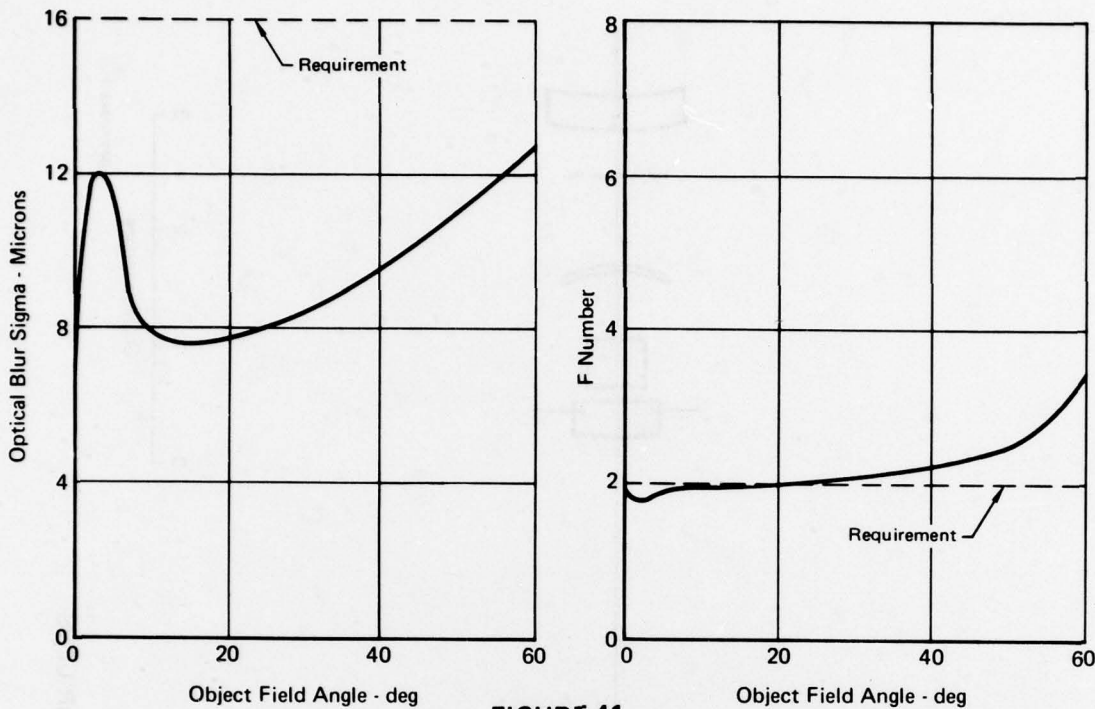
FIGURE 41

IR LENS PERFORMANCE

GP77-0348-4

may be somewhat better than these curves. However, because the blur on axis where high acuity viewing is accomplished is less than the 16 micron value, it should be noted that the 16 micron design value was a "not to be exceeded value" anywhere on the focal plane. Figure 41 showed that blur on axis was actually in the range of 8-12 microns with an average of 10 microns. The anticipated performance of this lens would be as shown by the dashed lines on Figure 42. The result is significantly better thermal resolution at all spatial frequencies. A comparison of thermal resolution at the human visual dynamic performance spatial resolution point (.86 $\frac{cycles}{mr}$) shows the performance improvements listed on Figure 43. The improvement is very substantial.

The analyses indicate narcissus is not a problem with current technology detectors and scanners. However, the larger cold assembly area and increased sensitivity of second generator detector arrays will necessitate some method of narcissus compensation.

No fabrication problems are anticipated with the design since all elements are made of germanium which can be easily ground to the relatively mild aspheric shapes required. Use of germanium also minimizes risk in both fabrication, coating, and homogeneity. Since these items are clearly within the state-of-the-art which is not true for many candidate materials.

The only problem with the design is the maintenance of an F/2.0 lens aperture at large field angles. Improvement made in the last few weeks of the contracted effort convinces us that further refinement in design can correct this problem. Work is continuing in this area on IRAD funds.

44

1. Serial, F/20 16μ, 488 Lines
2. Serial, F/2.0 10μ, 488 Lines
3. 2nd Gen, F/2.0 16μ, 481 Lines
4. 2nd Gen, F/2.0 10μ, 481 Lines

Human
Visual
Dynamic
Performance

GP77-0348-8
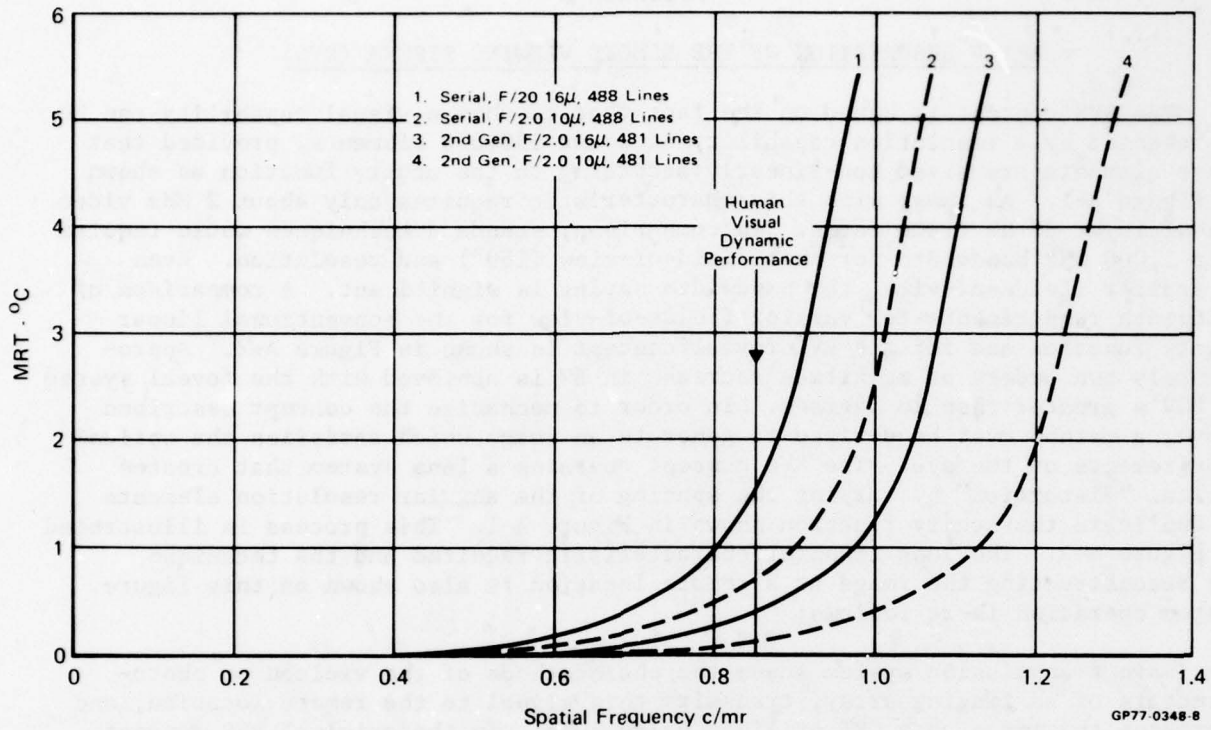
FIGURE 42
DETECTOR PERFORMANCE COMPARISON

Scanner Type	Optical Blur	
	16μ	10μ
Current Technology	1.6°C	0.6°C
Second Generation Technology	0.04	0.15

GP77-0445-2

FIGURE 43
MRT PERFORMANCE IMPROVEMENTS AT 0.86 C/MR
SPATIAL FREQUENCY BY REDUCING BLUR

Appendix A

BRIEF DESCRIPTION OF THE REMOTE VIEWING SYSTEM (RVS)

The RVS concept is based on the fact that the human visual capability can be represented by a resolution capability of about 130,000 elements, provided that these elements are sized non-linearly according to the acuity function as shown in Figure A-1. An image with this characteristic requires only about 2 MHz video bandwidth at 30 Hz frame rates. In comparison, standard techniques would require over 1,000 MHz bandwidth for this field-of-view (180°) and resolution. Even at smaller fields-of-view, the bandwidth saving is significant. A comparison of bandwidth requirements for varying fields-of-view for the conventional linear acuity function and for the RVS foveal concept is shown in Figure A-2. Approximately two orders of magnitude decrease in BW is achieved with the foveal system at FOV's greater than 20 degrees. In order to mechanize the concept described above, a method must be devised to generate an image which satisfies the optical requirements of the eye. The RVS concept contains a lens system that creates optical "distortion" by varying the spacing of the angular resolution elements to duplicate the acuity function shown in Figure A-1. This process is illustrated in Figure A-3. The lens transfer characteristic required and the technique for reconstructing the image at a remote location is also shown on this figure. System operation is as follows:

The image transmission system scans the photocathode of the vidicon or photo-detectors of an imaging array, transmits this signal to the remote location, and recreates the image on a CRT or light valve tube. In the original RVS concept, the distorted image is expanded using a lens system with a transfer characteristic identical to the sensor lens and imaged on a spherical screen concentric with the nodal point of the lens.

Obviously, for the above image transmission system to perform adequately, the optical axes of both the sensor and projector must have the same alignment as the viewer's eye. The initial RVS system concept used the approach outlined in Figure A-4. The position of the projector is slaved to the camera by a high accuracy position servo, with the camera's angular position commanding the projector's position relative to fixed ground station reference coordinates. The viewer at the ground station thus has the same angular perspective as he would if he were located in the remote vehicle. The sensor and projector must also be aligned with the viewer's foveal axis. In the original concept a Honeywell oculometer was employed for this function. The oculometer measures the angle between the eye's foveal axis and the projector's optical axis. This error signal is transmitted to the remote vehicle and commands the camera to move until the angular error is reduced to zero. As the camera moves, the projector follows through the slaving loop. The control mode, presently under study, is somewhat different, however. The observer's head position instead of his eye position is utilized to point the remote camera. The operational difference resulting from this simplification is that when the viewer uses his peripheral vision, he must learn to rotate his head towards the area of interest rather than his eyes. A reticle may be required to show the observer the location of the highest acuity area of the display.

Visual Field
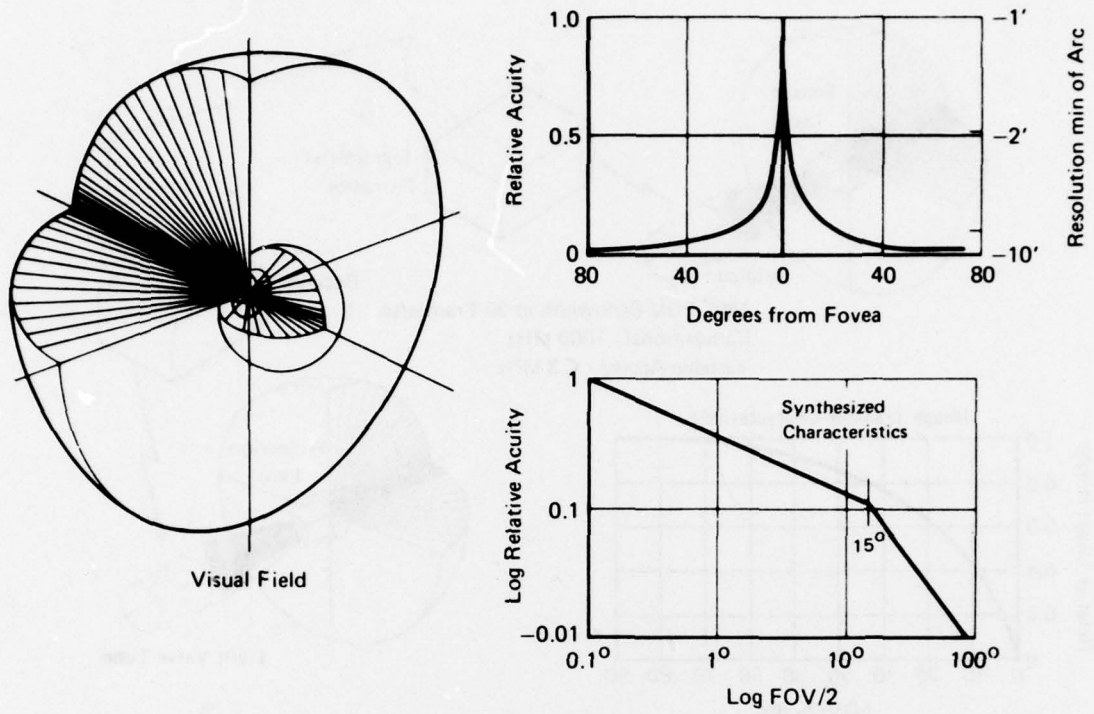
Figure A-1. Human Eye Characteristics

GP76-1037-112
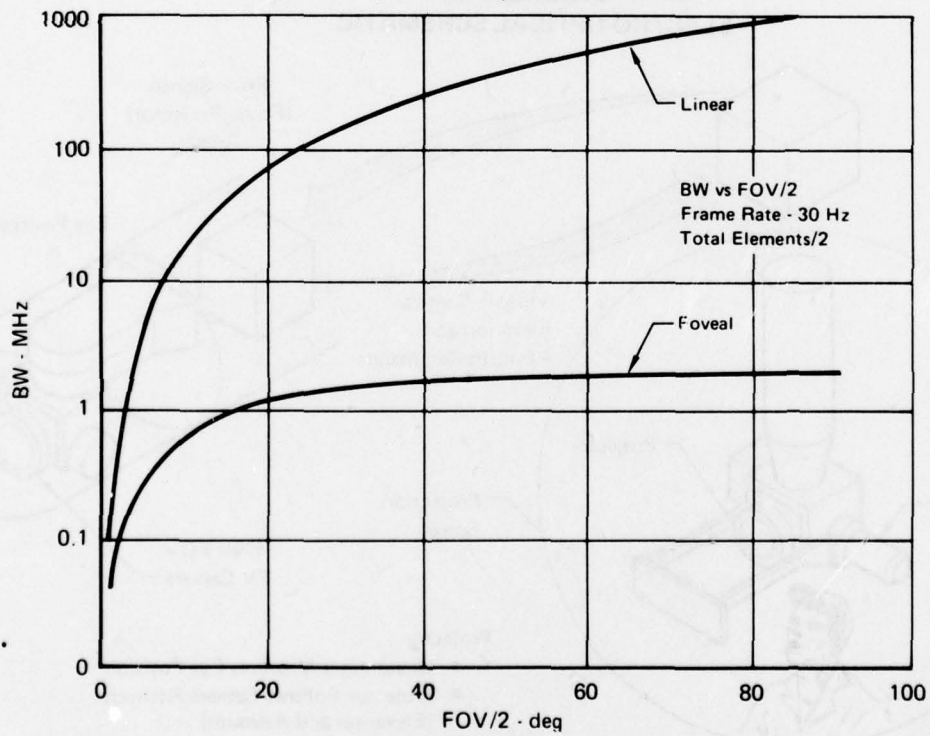
FIGURE A-2
BANDWIDTH REQUIREMENTS

GP76-1037-113

47
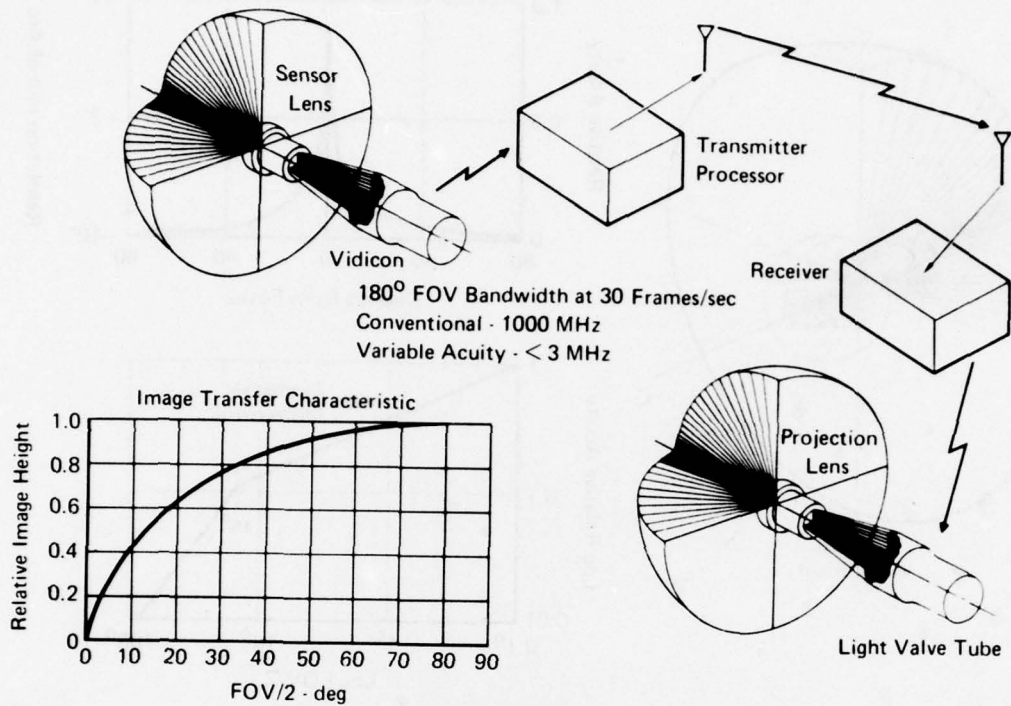
FIGURE A-3
ELECTRO-OPTICAL SCHEMATIC

Sensor Lens

Vidicon

180° FOV Bandwidth at 30 Frames/sec
Conventional - 1000 MHz
Variable Acuity - < 3 MHz

Transmitter Processor

Receiver

Projection Lens

Light Valve Tube

GP76-1037-110

Image Transfer Characteristic

FOV/2 - deg

Relative Image Height

Error Signals
(Fovea/Projector)
Angles

Eye Positions Camera

Video + Camera
Elevation and
Azimuth Commands

Oculometer

Projector

Projection Screen

Wide FOV
TV Camera

Projector
- Oculometer Measures Eye Position
- Projector Follows Camera Attitude
  (Elevation and Azimuth)

FIGURE A-4
CAMERA/PROJECTOR INTERFACE

GP76-1037-111

48

Appendix B

APPLICATION OF THE NIGHT VISION LABORATORY (NVL)
THERMAL VIEWING SYSTEM STATIC PERFORMANCE MODEL TO
THE RVS

4

It was suggested that the NVL Thermal Viewing System Static Performance Model be used to evaluate the performance of the Remote Viewing System (RVS). However, repeated attempts to convert the RVS parameters directly to the NVL model have led to the following problem. The radial distortion function of the foveal lens does not lend itself to an MTF analysis as a function of object field angular spatial frequency as called for in the NVL model. All parameters can be converted successfully except for the scan velocity term because a linear raster scan on the lens image plane will create a variable angular velocity and variable direction scan in the object field. This is depicted in Figure B-1. Extreme complexity results when attempts are made to convert spatial into temporal frequency. This is illustrated by the rotation of the f_x bar pattern in the lens image plane shown in Figure B-1. Given enough time, an analysis could be made in a manner compatible with the NVL model. However, the analysis is much simpler if performed, not in object field angular frequency (cycles/milliradian) but in spatial frequency terms (lines/millimeter). For our purpose of optimizing the RVS lens, it is simpler to work in terms of spatial frequency on the foveal lens focal plane.

This simplicity arises because seven of the nine MTF's are independent of object field angle at this foveal lens focal plane location, and the scan velocity is undirectional and uniform at this location, thereby making easy conversions from spatial to temporal parameters. The only non-linear conversions necessary are simple geometrical ones which translate from focal plane to object field and display space. The advantages of working in the spatial frequency terms will become clear as the analysis is developed. In the following development, the NVL model approach will be used precisely but will be applied in the foveal lens focal plane as a function of linear spatial frequency (1/mm). Parameters will be covered in the same order as they are in the NVL Report [4], which describes the model in detail.

B.1 MTF's

1. Optical MTF The optical MTF's consist of a diffraction MTF and a Gaussian MTF.
(a) Diffraction In angular terms, the diffraction MTF is referenced as Equations (9) and (10) of the NVL report:

$$H_{opt}(f_x, \theta) = \frac{2}{\pi} \left[\cos^{-1} A - A(1 - A^2)^{1/2} \right] \qquad (B-1)$$

$$\text{where} \qquad A = \lambda F_{\#} f_x / L(\theta) \qquad (B-2)$$

where $L(\theta)$ is the equivalent focal length which changes over a 50/1 range as object field angle θ changes. The angle θ is the absolute angle between the point of interest and the lens optical axis. At the foveal lens image plane

$$S_x = \frac{f_\mu}{L(\theta)} \qquad (B-3)$$

49

(b) <u>Blur</u> - A similar simplicity exists here. The MTF equation with the angular term b of Equation (11) of Reference(B-1)replaced with its equivalent is:

$$H_{blur}(f_x, \theta) = \exp\left[-\frac{2\pi^2 \sigma^2}{L(\theta)^2} f_x^2\right] \tag{B-7}$$

The foveal lens inherently has a constant spatial blur over its entire focal plane, so that the sigma (σ) of Equation(B-7)is a constant. Substituting Equation(B-5)into (B-7) we see the blur MTF simplifies to

$$H_{blur}(S_x) = \exp\left[-2\pi^2 \sigma^2 S_x^2\right] \tag{B-8}$$

Thus this MTF like the diffraction MTF, is no longer a function of object field angle because the focal length variable has been removed.

2. <u>Detection MTF</u> - The spatial filter MTF of the detector is defined as:

$$H_{Det}(f_x, \theta) = \frac{Sin(\pi f_x \Delta x)}{\pi f_x \Delta x} \triangleq Sinc(f_x \Delta x) \tag{B-9}$$

It is also complex in our system because the angular projection of the detector into the object field (Δx) in this equation varies with absolute object field angle (θ). Since the detector height is still uniform at the lens focal plane, shown in Figure(B-2)as Δh, Equation(B-9)can be restated as:

$$H_{Det}(S_x) = \frac{Sin(\pi S_x \Delta h_x)}{\pi S_x \Delta h_x} \tag{B-10}$$

Again the MTF becomes independent of object field angle. Note from Figure(B-2)that the detector height (Δh_x) is a function of detector size(a), detector system focal length (L_D), and relay focal length (L_C), viz:

$$\Delta h_x \approx a_x \frac{L_C}{L_D} \tag{B-11}$$

There are two ways to arrive at the required L_C and L_D based upon whether the scanner or detector characteristics are known. If the scanner is available, horizontal FOV (θ_s) and instantaneous FOV (α) are known. Then the detector focal length is

$$L_D = \frac{a_x}{\alpha_x} = \frac{a_y}{\alpha_y} \tag{B-12}$$

50
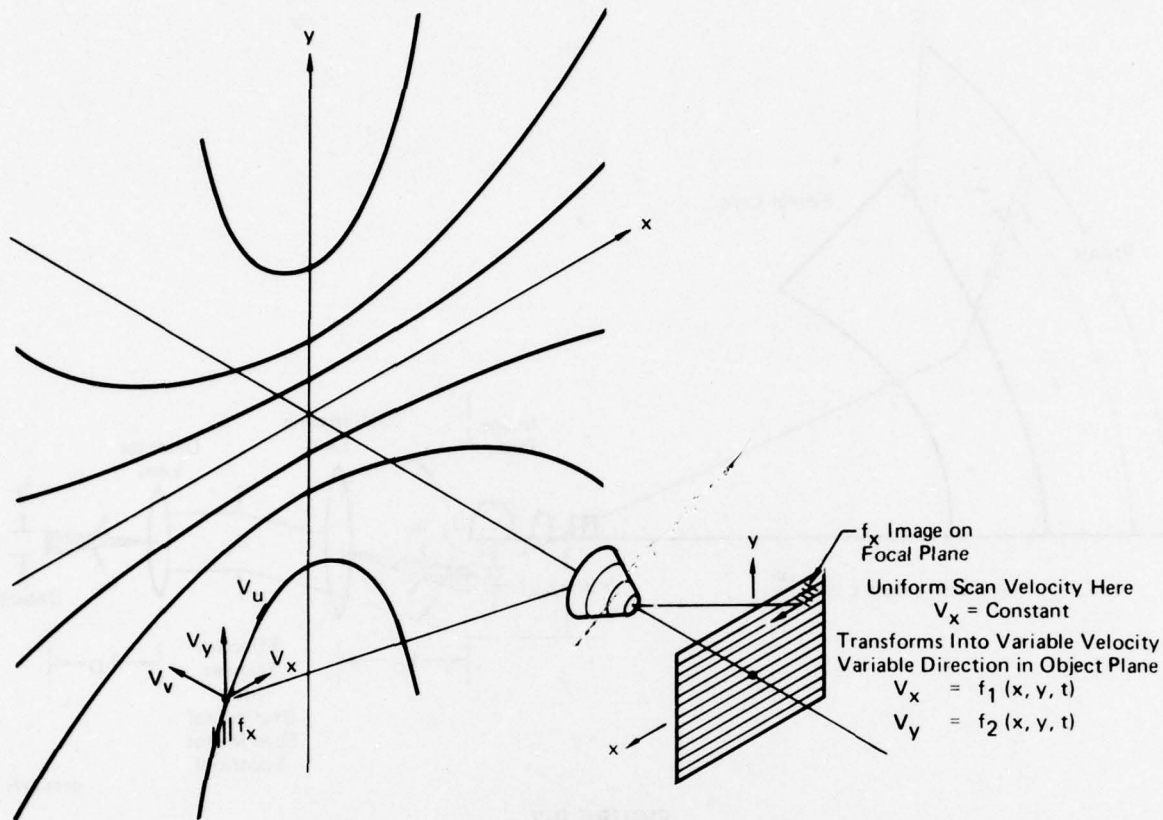
FIGURE B-1
SCAN DISTORTION INTRODUCED BY FOVEAL LENS

GP76-1037-109

where S_x is the image plane spatial frequency and f_μ is its object field angular equivalent measured along the scan line projection in the object field (μ direction on Figure B-1). Solving for f_μ in Equation (B-3) and substituting this for f_x in Equation (B-2).

$$A = \lambda F_{\#} S_x \tag{B-4}$$

Since the F/number of our lens is constant, the diffraction MTF is no longer a function of object field angle. Thus we may write $H_{opt}(S_x)$ which indicates that the MTF is a function of the independent variable S_x only. Note, however, that conversion to object field angular spatial frequency is very simple because focal length is constant over small angular increments and may be determined from

$$f_\mu = S_x L(\theta) \tag{B-5}$$

where μ is along the scan line projection in the object field

likewise

$$f_w = S_y L(\theta) \tag{B-6}$$

where w is normal to the scan direction in the object field

51
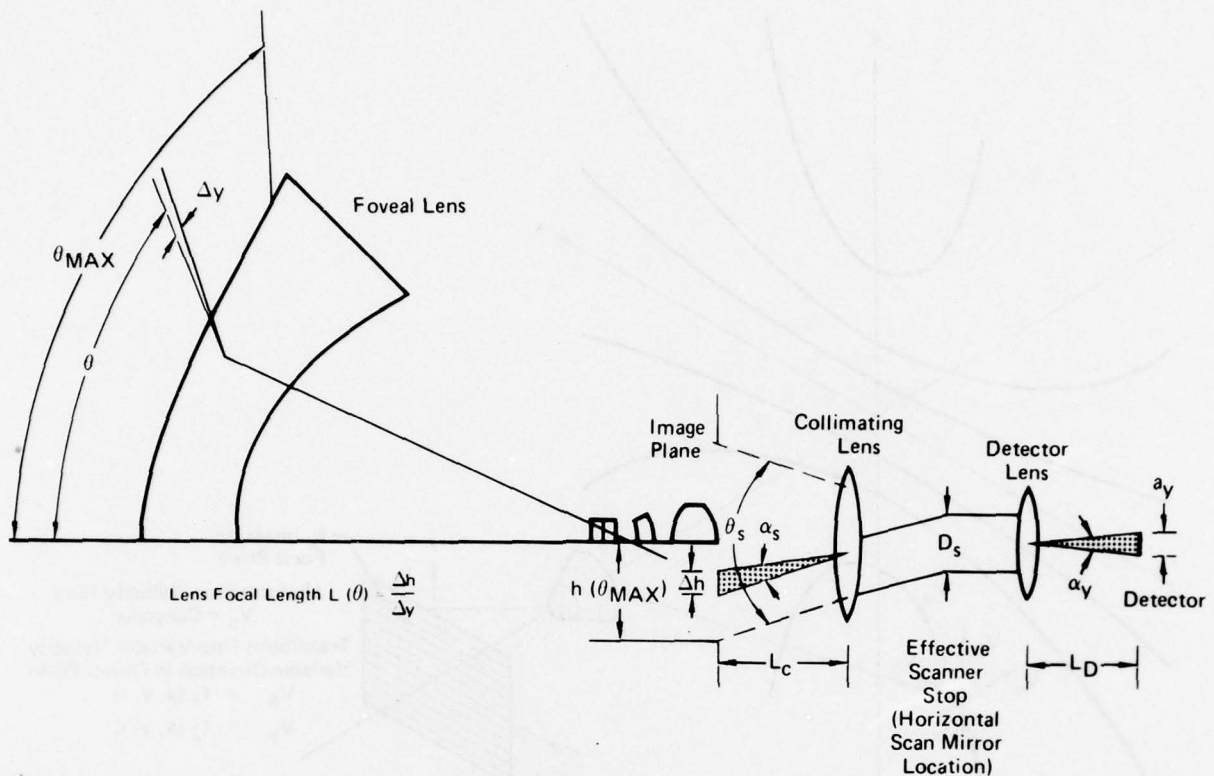
FIGURE B-2
SCANNER RESOLUTION ELEMENT GEOMETRY

On the forward end of the scanner we must cover the foveal lens image plane height of $2h(\theta_{max})$ which subtends the angle θ_s. Thus,

$$\frac{h(\theta_{max})}{L_C} = \tan \frac{\theta_s}{2} \qquad (B-13)$$

Solving for L_C

$$L_C = \frac{h(\theta_{max})}{\tan \theta_s/2} \qquad (B-14)$$

If the detector characteristics are known, the focal lengths are a function of detector size (Δh) projected unto the image plane as shown in Figure (B-2). Detector size Δh can be computed directly from either the on-axis resolution required, the number of scan lines required across the vertical FOV, or bandwidth/response restrictions and frame rate requirements. The focal lengths, L_C and L_D, are then selected to make the detector dimension appear as the required Δh at the foveal lens focal plane. The scanner horizontal FOV given by scanner mechanics must cover the total image plane height $(2h(\theta_{max}))$. In either case the detector

52

MTF becomes:

$$H_{Det}(S_x) = \text{Sinc} \frac{a_x \, L_C}{S_x \, L_D} \qquad (B-15)$$

Again this MTF is independent of object field angle.

3. <u>Detector Electronics MTF</u> - It is in the MTF, the detector electrical response, that we get into real trouble trying to work in object field angular space. For a conventional linear optical system, a linear detector scan velocity converts into a scaled but linear angular scan in the object field. This is not true in our system as was shown in Figure B-1. A linear scan in the x direction on the image plane results in angular velocities in both θ_x and θ_y directions in the angular object field. Both of these angular components are nonlinear functions of both x and y position on the image plane. Thus, converting from spatial frequency to temporal frequency becomes very complex. All of this can be avoided by working in linear spatial plane terms. If the scanner has an angular scan velocity β, then the linear motion of the instantaneous FOV on the foveal lens image is

$$V_x = \beta L_C \qquad (B-16)$$

The conversion to temporal frequency (f) is therefore

$$f = V_x \, S_x \qquad (B-17)$$

This is a constant conversion and not a function of time. Therefore, all electronic MTF's of the NVL model are valid. These are

$$H'_{Det}(f)$$

$$H_{Elect}(f)$$

$$H_B(f)$$

4. <u>Display</u> - The RVS display is the inverse of the foveal lens, which results in a conventional linear raster generated on the CRT. The CRT has a constant spot size and the expansion optics has a constant blur at the object focal plane. Again this MTF, if derived in the linear spatial plane, will not be a function of object angle. If the optical blur and CRT spot size are combined and assumed to have a Gaussian MTF, a composite sigma (σ_d) results and the MTF is:

$$H_{Disp}(S_x) = \exp\left[-2\pi^2 (r\sigma_d)^2 S_x^2\right] \qquad (B-18)$$

where r is the physical ratio of format sizes; viz

$$r = \frac{H_{LENS \; IMAGE}}{H_{DISPLAY \; CRT}} \qquad (B-19)$$

53

By contrast, if this were accomplished in the object angular plane, the MTF would be much more complex, viz

$$H_{Disp}(f_{x,\theta,M}) = \exp\left[-\frac{2\pi^2(r\sigma_d)^2 f_x^2}{L(\theta)^2 M^2}\right] \tag{B-20}$$

where M is any system angular magnification from object field to the viewer. Again the simplicity is obvious.

5 & 6. <u>Stabilization and Eyeball</u> - The remaining two MTF's are the only two that are not simplified by working in linear spatial rather than angular terms. First, stabilization tends to be angular input to the system. Using the MTF from the NVL report:

$$H_{Los}(f_x) = \exp(-Pf_x^2) \tag{B-21}$$

Converting to the foveal lens image plane results in

$$H_{Los}(S_{x,\theta}) - \exp\left[-PS_x^2 L(\theta)^2\right] \tag{B-22}$$

Similarly, the eye views the display in angular terms. The NVL MTF is

$$H_{Eye}(f_x) = \exp\left[-\frac{\Gamma f_x}{M}\right] \tag{B-23}$$

Equation (B-23) must be converted to the foveal lens image plane

$$H_{Eye}(S_{x,\theta}) = \exp\left[-\frac{\Gamma S_x L(\theta)}{M}\right] \tag{B-24}$$

In conclusion, seven MTF's have been simplified at the expense of two that have been made slightly more complex by the conversion to linear spatial frequency.

B.2 NEΔT

NEΔT can be used as defined in the NVL document since it is independent of spatial frequency, therefore no changes are required. However, it is a function of F/number and a discussion is in order concerning which is the correct F/number to use in the calculation. It is not simply the foveal lens F/number or objective lens F/number as stated in the NVL document. For NEΔT calculations, the F/number must represent the actual ray cone supplying the detector.

In general our lens will be limited to a fixed image height $h(\theta_{max})$ that is based on fabrication considerations. The scanner must cover this total image in the most efficient manner. The optical geometry of the lens and scanner can be reduced to the basic arrangement shown in Figure (B-3). On this figure the ray cone that supplies the detector is ϕ_4. Note that a maximum ray cone (ϕ_3) that the detector can utilize exists. Obviously,

FOVEAL LENS

SCANNER

Lens - Focal Length, $L(\theta) = \dfrac{dh}{d\theta}$

Effective Entrance
Pupil Diameter, $D(\theta) = \dfrac{L(\theta)}{F\#}$

$F\# = $ Constant

GP76-0773-3
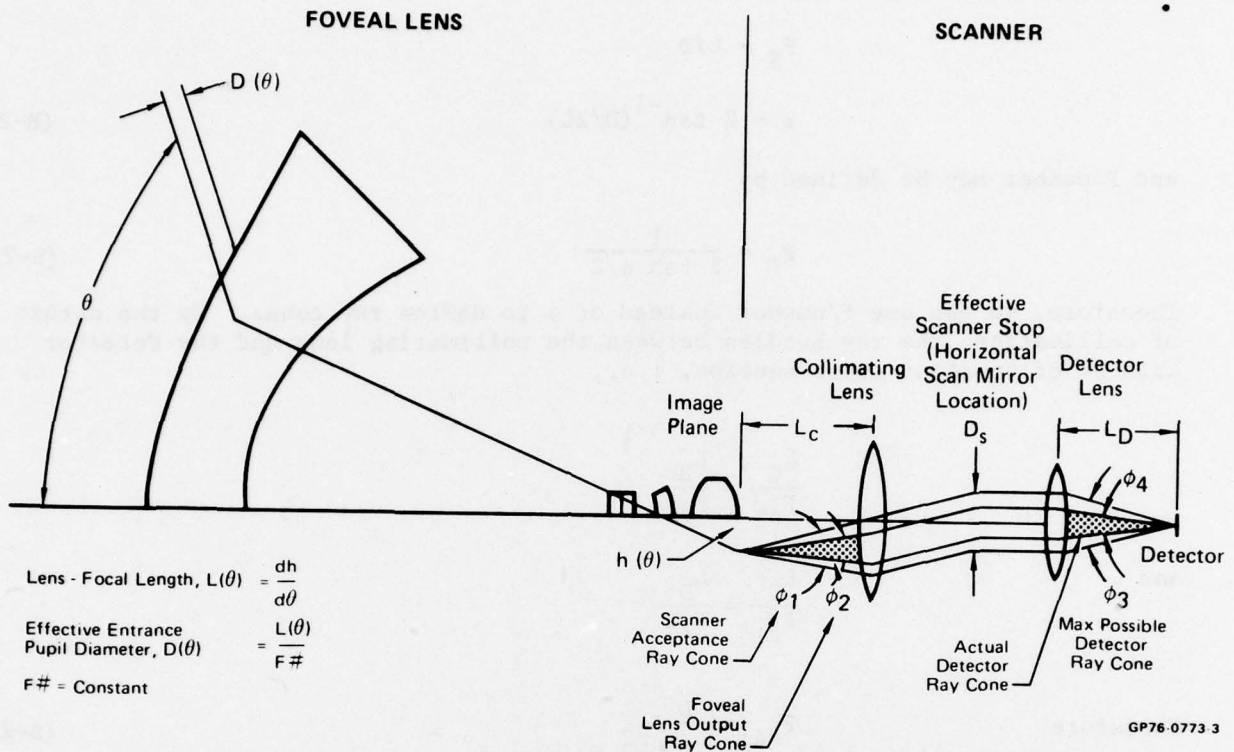
**FIGURE B-3
GENERAL LENS/SCANNER GEOMETRY**

the best design would have $\phi_3 = \phi_4$. This is not always possible, however, because the lens may be required to operate with available scanners. Therefore, it will be necessary to define both of these ray cones and utilize the smallest for NEΔT and diffraction MTF calculations. Before processing, note that ray cones may also be defined by F/numbers as shown in Figure (B-4).

GP76-0773-4
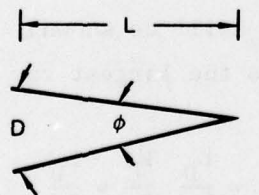
Figure B-4. Ray Cone Parameters

Since anywhere along the ray bundle

$$F_{\#} = L/D$$

$$\phi = 2 \tan^{-1}(D/2L) \tag{B-25}$$

and F/number may be defined by

$$F_{\#} = \frac{1}{2 \tan \phi/2} \tag{B-26}$$

Therefore, we can use F/number instead of ϕ to define ray cones. By the nature of collimation, the ray bundles between the collimating lens and the detector will be of constant cross section, i.e.,

$$\frac{L_C}{F_{\#2}} = \frac{L_D}{F_{\#4}}$$

And

$$\frac{L_C}{F_{\#1}} = \frac{L_D}{F_{\#3}}$$

Therefore

$$F_{\#4} = \frac{L_D}{L_C} F_{\#2} \tag{B-27}$$

And

$$F_{\#3} = \frac{L_D}{L_C} F_{\#1} \tag{B-28}$$

The larger of these two F/numbers must be used for both diffraction and NEΔT calculations. Now note that $F_{\#2}$ is the F/number of the foveal lens while $F_{\#1}$ is that generated by the scanner internal aperture stop (D_s) and we may write:

$$F_{\#1} = \frac{L_C}{D_S} \tag{B-29}$$

For any particular scanner, D_s will be known. From Equation (B-28) the smallest F/number which translates into the largest ray cone we can supply the detector with is:

$$F_{\#3} = \frac{L_D}{L_C} \frac{L_C}{D_s} = \frac{L_D}{D_s} \tag{B-30}$$

which is also obvious from inspection.

.

56

For our ONR work, a scanner has been specified while for the USAF effort only a detector geometry is available. The following derivations will try to accommodate both arrangements. If the scanner is specified, D_s and L_D will be known. If L_D is not given it can be calculated from the scanner instantaneous FOV (α) and detector size (a) in the same plane. Then

$$L_D = \frac{a_y}{\alpha_y} \qquad (B-31)$$

Also, if the scanner is specified, its maximum scan angle (θ_s) shown in Figure (B-2) is known. Since the scanner must scan the entire image, θ_s must cover $2h(\theta_{max})$. Then

$$L_C = \frac{h(\theta_{max})}{\tan \frac{\theta_s}{2}} \qquad (B-32)$$

It is now possible to compute $F_{\#4}$ from Equation (B-27).

$$F_{\#4} = \frac{a_y \tan \theta_s/2}{\alpha_y h(\theta_{max})} = F_{\#2} \qquad (B-33)$$

where $F_{\#2}$ is the foveal lens F/number. Remember, for the diffraction MTF and NEΔT calculations, we use the larger of $F_{\#4}$ or $F_{\#3}$.

If a scanner is not defined, one must be theorized. This can easily be accomplished by procedures outlined in Lloyd [B-1]. Generally, scanning hardware (mirror, drum, etc.) are selected to accomplish a given scan angle θ_s (number of facets). Collimation lens focal length (L_C) can then be computed by Equation (B-32). From the required scan lines across the maximum image height $h(\theta_{max})$, the apparent detector size (Δh) at the image can be calculated. The angular instantaneous FOV of the scanner can be calculated as follows, using the on-axis geometry of Figure (B-2):

$$\alpha_y = \frac{\Delta h}{L_C} \qquad (B-34)$$

L_D can then be calculated by

$$L_D = \frac{a_y}{\alpha_y} \qquad (B-35)$$

D_s can then be defined by matching the lens F/number

$$D_s = \frac{L_C}{F_{\#}} \qquad (B-36)$$

57

B.3 MRT CALCULATIONS

The following MRT equation modifications are required so that the computation may be performed in linear spatial frequency terms. First, in the NVL MRT equation, Δy must be replaced by the apparent detector size at the foveal lens image plane, i.e., it must be the Δh defined on Figure (B-2). As previously demonstrated in Equation (B-11),

$$\Delta h_y = a_y \frac{L_C}{L_D} \qquad (B-37)$$

Also, in the MRT equation, it is best to compute the Q integral in terms of temporal frequency. This eliminates the velocity term in the MRT equation and makes the Q integral easier to compute. The Q integral is therefore

$$Q(f,\theta) = \int_0^\infty \frac{S(f)}{S(f_o)} H_N^2(f) H_w\left(\frac{f}{V_x}\right)^2 H_{Eye}\left(\frac{f}{V_x}\right) df \qquad (B-38)$$

Of these terms, only H_w, the transfer function for a rectangular bar of width w, has not been defined. This transfer function is in linear rather than angular dimensions, i.e.,

$$H_w\left(\frac{f_x}{V_x}\right) = \text{Sinc}\left(W \frac{f_x}{V_x}\right) = \text{Sinc}\left(WS_x\right) \qquad (B-39)$$

where

$$W \triangleq \frac{1}{2S_x} \qquad (B-40)$$

The MRT equation written to show the dependency of two variables is

$$MRT(S_x,\theta) = \frac{SNR\pi^2 NE\Delta T}{4\sqrt{14}\ MTF_{TOTAL}(S_x,\theta)} \left[\frac{\Delta h_y\ S_x Q(f,\theta)}{\Delta f_N F_R\ t_e\ \eta_{OVSC}}\right]^{1/2} \qquad (B-41)$$

This equation results in an MRT very weakly dependent on θ. To obtain the MRT for any field angle θ we convert the spatial frequency term S_x into an angular frequency term by using Equation (B-5) containing the focal length function:

$$f_\mu = S_x L(\theta) \qquad (B-5)$$

Note this will be the angular spatial frequency in the scan direction (target bars normal to the scan direction). It could be related to f_x and f_y but this does not appear to be required at this point.

Appendix C

THEORY OF NARCISSUS ANALYSES

The problem of the IR detector "seeing" cold focal plane surfaces which are reflected by the system optics in addition to the warm target is labeled the "Narcissus Problem". The source of the narcissus problem is illustrated in Figure C-1. In Figure C-1 the detector assembly is shown at the center scan position. All areas of the rear clear aperture of the optics are flooded with photons emitted from the 300°K structure surrounding the detector assembly. Most of these photons are absorbed by the lens structure or pass out into the object field. A small number however, are reflected back to the image plane by the various lens elements and therefore some of these returning photons fall on the detector to alter its electrical output. Alternatively, the emitted photon flux field from the warm structure may be thought of as being disrupted by the cold detector assembly which for all practical purposes has no emission. Therefore a cold "hole" is introduced into the flux field. The narcissus problem is generated when this hole is made to translate across the optical image as illustrated by the dashed lines in Figure C-1. This occurs during the mechanical scanning. This translating region of non-emission will cause a fluctuation in the reflected photon distribution at the detector plane. If this spatial fluctuation is smaller than the total scan, an unwanted signal will be generated during the scan. The generation and prediction of the narcissus image are described below.

The best way to compute significance of the "narcissus" energy is to assume that the detector cold assembly is emitting at 300°K and trace the reflections that return to the detector plane. The spatial distribution of reflected portion of this energy in the detector plane is the photon energy that will be absent in the actual situation, hence, a "cold" output will be obtained from the detector. This process is shown in Figure C-2.

At the "start scan" position shown in Figure C-2(a), three points of emission on the detector cold assembly are shown. In the most severe situation (negative magnification) the reflected energy will appear on the opposite end of the scan. For example, if the optics are theorized to form an image somewhat in front of the focal plane by reflection, the three ray bundles will converge forward of the focal plane and expand towards the focal plane. This energy forms a "blur" area in the focal plane as shown in Figure C-2(a). Remember this area represents a region of "less photons" than the surrounding area. Since the detector does not lie within this area, its output is not influenced by it.

In Figure C-2(b) the detector cold assembly is shown at 1/4 scan. Note that here the "narcissus" image has moved towards the detector but still has not influenced its output. In Figure C-2(c) the detector is shown at center scan. Here it lies directly within the "narcissus" area and will, therefore, have less output or will have a cold output created by the lower photon input. As the detector completes the scan, it moves outside of the "narcissus" area as shown in Figure C-2(d) and is no longer affected by narcissus. The total result then is a "cold" image resembling the narcissus blur area at the center of the FLIR display. This is illustrated in Figure C-3.

To compute the true effect of narcissus, a ray trace of all points within the detector cold assembly should be conducted. Sufficient ray tracing must be conducted to map the power density in the detector plane. Much of this laborious procedure can be avoided by a series of simplifications. For example, if the portion

59
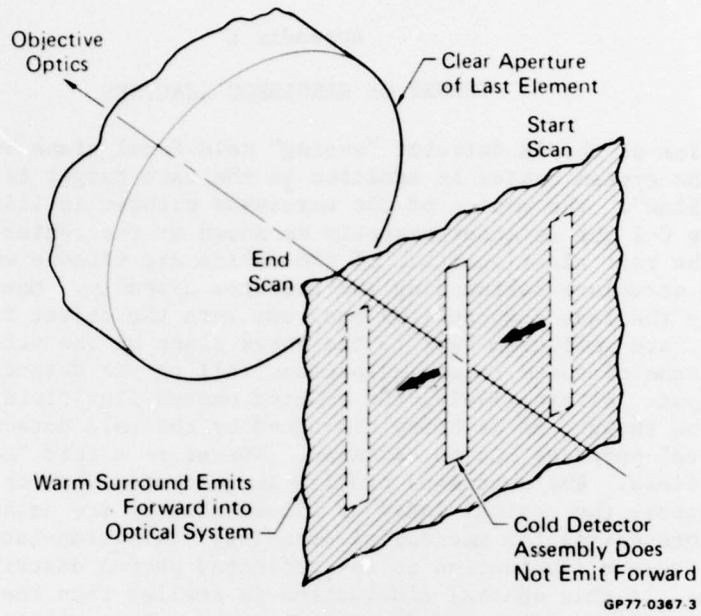
Figure C-1. Source of Narcissus Energy

GP77-0367-3

a. Start Scan

b. 1/4 Scan

c. Half Scan

d. 3/4 Scan

*For analysis purposes only. The Cold Detector does not emit. The background would emit this energy if detector assembly was absent.
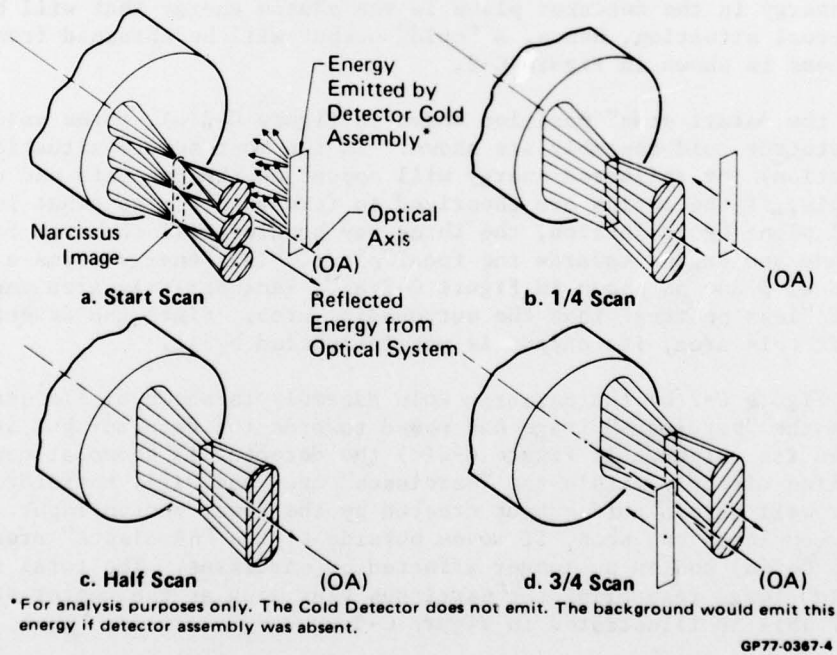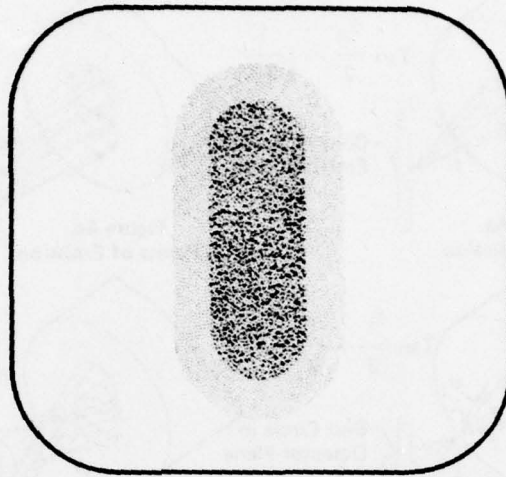
GP77-0367-4

FIGURE C-2
NARCISSUS IMAGE GENERATION

GP77-0367-5

FIGURE C-3
NARCISSUS DISPLAY OF FIGURE C-2

of the narcissus image that contributes to illumination of the on-axis detector can be established, simple optical and radiometric theory can be utilized to define the maximum strength of the narcissus effect. A similar procedure can be used to estimate the size of the narcissus image. This is developed in the following paragraphs.

On Figure C-4(a), emission of the on-axis point of the cold assembly is illustrated. If narcissus analysis is being performed on a surface forward of the scan mechanism, the only energy that will be reflected back to the detector is confined within the F/number cone of detector. This cone is defined by the basic optical design. From elementary geometric optics, the energy returning from the forward surface will be confined to this cone but altered by the optical magnification. With reference to Figure C-4 it is easily seen that the blur circle radius is:

$$R = S \tan \frac{\theta i}{2} = \frac{S}{2 \ M \ FNo} \tag{C-1}$$

where S = Distance narcissus image is in front of detector plane
       M = Magnification

The above are shown in Figure C-4(a) and (b) and is the narcissus power contribution for a single point on the cold emitting assembly. Obviously, the detector will be affected by the integrated results of the emission of all points on the cold assembly that can pass through the optical system and be reflected back to the detector. Three of these are shown in Figure C-4(c). It is easily seen that all of these points contribute to output of the detector located near the optical axis. The difficult task is to estimate just how much of narcissus image is capable of illuminating the detectors. This is a function of direction of the chief rays forming the narcissus image.

In Figure C-5 the image cone of the on-axis detector is shown. For a correctly designed optical system, it will be impossible for any returning ray to reach the on-axis detector unless it falls within this cone. Therefore, rays forming the

61

$$\text{Tan} \frac{\theta_o}{2} = \frac{1}{2 \, FNo}$$

Cold Assembly
Emitting Area

Figure 4a.
on Axis Emission

Figure 4c.
3 Points of Emission

$$\text{Tan} \frac{\theta_i}{2} = \frac{1}{M} \text{Tan} \frac{\theta_o}{2}$$

Blur Circle in
Detector Plane

$$\text{Radius } R = \frac{S}{2 \, M \, FNo}$$

Detector Area
Influenced by All
Three Points

Figure 4b.
Narcissus Image

Figure 4d.
Integrated Blurs at Detector
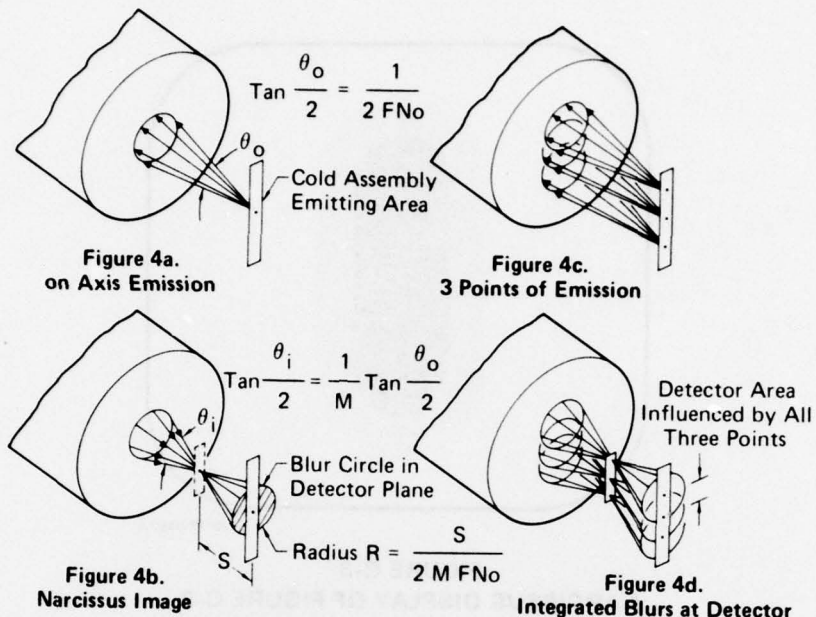
GP77-0367-6

FIGURE C-4
NARCISSUS BLUR CIRCLE RADIUS

$N = 300°K$ Radiance of Detector Cold Assembly
τ = Optical Transmission Reflectance Product
τN = Radiance of Narcissus Image
W_D = Detector Area/$S^2 = A_D/S^2$
$P_D = \tau N A_i \, W_D$

$$P_D = \frac{4\tau \, N A_D XY}{S^2}$$

Narcissus Image Area that
can Illuminate an On-Axis
Detector $A_i = 4 \, x \cdot y$

Where:

$$y = \frac{S}{2 \, FNo} \text{ or } M \frac{a_{cay}}{2} \text{ Whichever is Smaller}$$

$$x = \frac{S}{2 \, FNo} \text{ or } M \frac{a_{cax}}{2} \text{ Whichever is Smaller}$$

In Most Cases

$$P_D = \frac{\tau N A_D \, M \, a_{cax}}{S \, FNo}$$
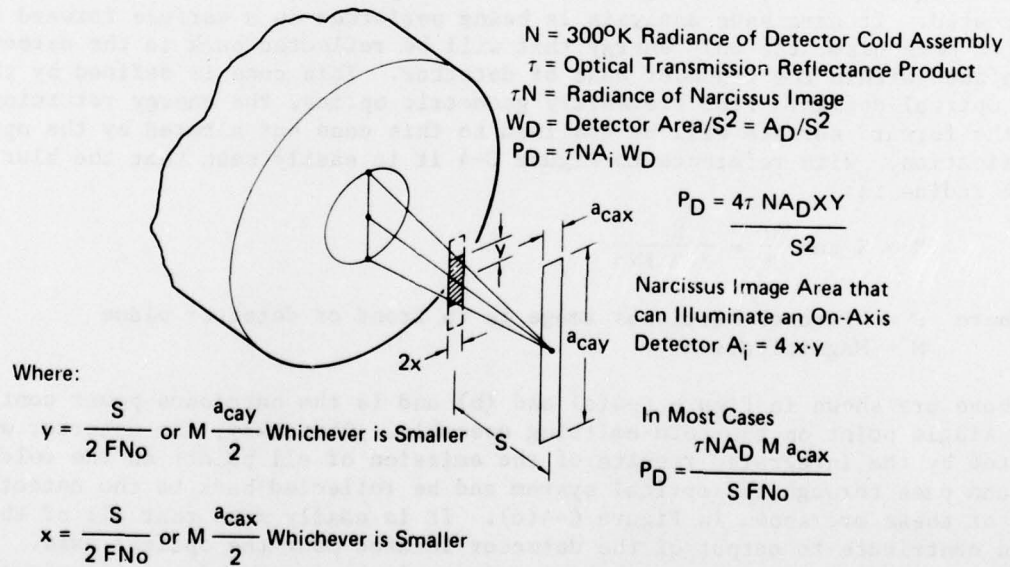
GP77-0367-7

FIGURE C-5
ON AXIS NARCISSUS POWER CALCULATION

narcissus image cannot illuminate this detector if they occur farther from the optical axis than the distance y on Figure C-5. The narcissus area (A_i) on Figure C-5 is therefore

$$A_i = 4 \times y \qquad \text{(C-2)}$$

Now employing another simple optical theory, that the image radiance (N_i) is numerically equal to the object brightness (N) times an attenuation factor T, which is the product of all transmissions and reflectances throughout the narcissus path. The derivation of the on-axis power equaiton is shown on Figure C-5. For a linear array, the last equation almost always applies, i.e.:

$$P_D = \frac{T \, N \, A_D \, M \, a_{cax}}{s^2} \qquad \text{(C-3)}$$

Unfortunately on-axis power is not sufficient to fully assess the significance of narcissus. The spatial structure on the display must be known, because in many cases the narcissus power may be many times the detector NEP but its influence may cover all detectors equally during scan. Therefore it will not be seen. This is especially possible if positive magnification exists.

Starting with the more simple case of negative magnification, the case depicted on Figure C-2, estimation of narcissus image size is very easy. For $S > a_{cax}$, the blur image width (w) in the detector plane is

$$w = 2R = \frac{S}{M \, FNo} \qquad \text{(C-4)}$$

The velocity of this blur during scan is

$$V_{blur} = MV. \qquad \text{(C-5)}$$

Since the detector moves in the opposite direction with velocity V, the relative velocity between the two is

$$V_r = V(1 - M) \qquad \text{(C-6)}$$

The time required to scan the narcissus image is

$$t_{blur} = \frac{2R}{V_r} = \frac{2R}{V(1-M)} \qquad \text{(C-7)}$$

The time required to scan the total format is

$$t_s = \frac{X}{V} \qquad \text{(C-8)}$$

where X is format width

The ratio of the display width covered by the narcissus image is

$$r = \frac{t_{blur}}{t_s} = \frac{2R}{(1-M)x} \qquad \text{(C-9)}$$

For positive magnification, the theory is much more complex. First it is necessary to know the nature of the basic image to proceed with this calculation. For a telecentric image (all chief rays parallel to the optical axis). The theory

63

can be developed as follows. Figure C-6 must be used for this derivation. This figure is a view in the x plane. Therefore the detector and Narcissus image are vertical lines normal to the paper that move from the bottom of the page (start scan) to the top (end scan). In this case (positive magnification), the narcissus image goes in the same direction as the detector, and may continue to illuminate all detectors throughout the scan, unless vignetting occurs within the optical system. Again, by assuming a telecentric optical image, an assessment can be made of this effect on the displayed image. In this case the optics will limit narcissus rays to the format diagonal dimension on the detector plane because the optics were designed to do this. This means that no ray can rise higher than the height (W) in the narcissus image plane, again remembering that moving vertical pencils are being considered. In this case, the narcissus energy will be completely vignetted when the detector array is at a height $(\frac{W}{M})$ from the optical axis. It seems logical therefore, to assume the image disappears at this point. The derivation shows that for this assumption the ratio of narcissus occupied display format height is:

$$r\ (S) = \frac{1.41}{M} + \frac{S}{M\ a_{cay}\ FNo} \tag{C-10}$$

A similar analysis for negative values of S yields

$$r\ (-S) = \frac{1.41}{M} - \frac{S}{M\ a_{cay}\ FNo}$$

$$W = \frac{\sqrt{x^2 + y^2}}{2} + \frac{S}{2\ FNo}$$

Narcissus not Present when Scan Reaches Height $\frac{W}{M}$, Therefore

If:

$$X = Y = a_{cay}$$

$$r = \frac{W}{MX} = \frac{\sqrt{x^2 + y^2} + \frac{S}{FNo}}{MX}$$

$$r = \frac{1.41\ a_{cay} + \frac{S}{FNo}}{M\ a_{cay}}$$

$$r = \frac{1.41}{M} + \frac{S}{M\ a_{cay}\ FNo}$$
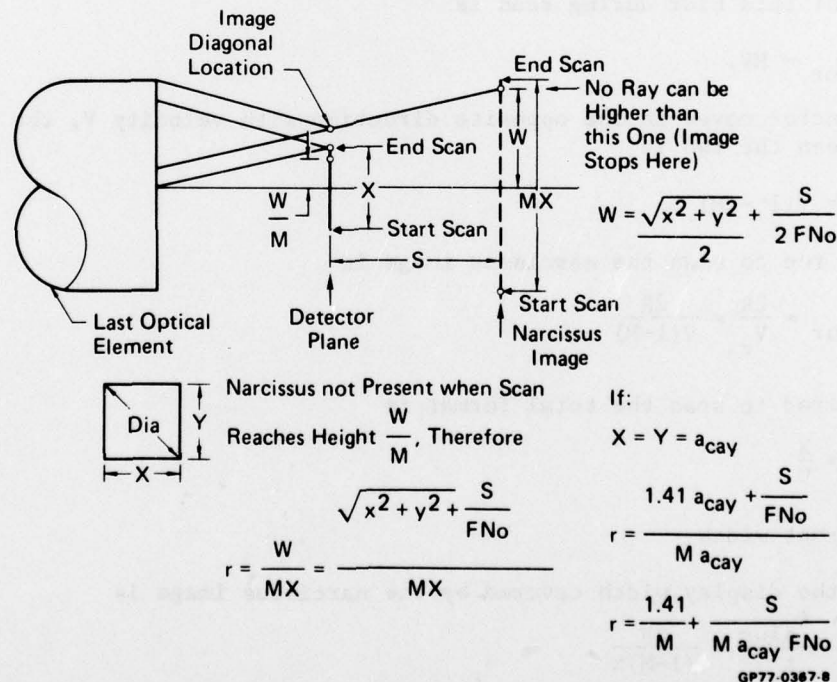
GP77-0367-8

FIGURE C-6
NARCISSUS SIZE FOR POSITIVE MAGNIFICATION

64

Appendix D

NONLINEAR LENS F/NUMBER DETERMINATION

The derivation of the F/number of the nonlinear lens is defined in this Appendix. Germaine terms are defined on Figure D-1. Photons are radiated from the earth (or target) at a slant distance (S) and radial distance (R) from the nonlinear lens. The variables S and R are much greater than the clear aperture diameter (DCA). This photon flux is specified by a radiance (N) in watts/CM^2-Steradian. For an infinitesimal area in the object field (A_t), the power (P_a) entering the lens pupil of area (A) is:

$$P_a = NA_t W \qquad (D-1)$$

where ω = Solid angle subtended by the entrance pupil $\qquad$ (D-2)

$$\omega = \frac{A}{S^2}$$

Then

$$P_a = \frac{NA_t A}{S^2} \qquad (D-3)$$

This entire flux must appear on the lens image plane within the image (A_i) of object area (A_t).

$$A_i = dt\ dr$$

The power density of the focal plane is therefore

$$W = \frac{P_a}{A_i} = \frac{NA_t A}{S^2\ dt\ dr} \qquad (D-4)$$

Now A_t can be related to the image plane through lens focal length. By definition the radial focal length (f_r) is

$$f_r(\theta) = \frac{dr}{d\theta} \qquad (D-5)$$
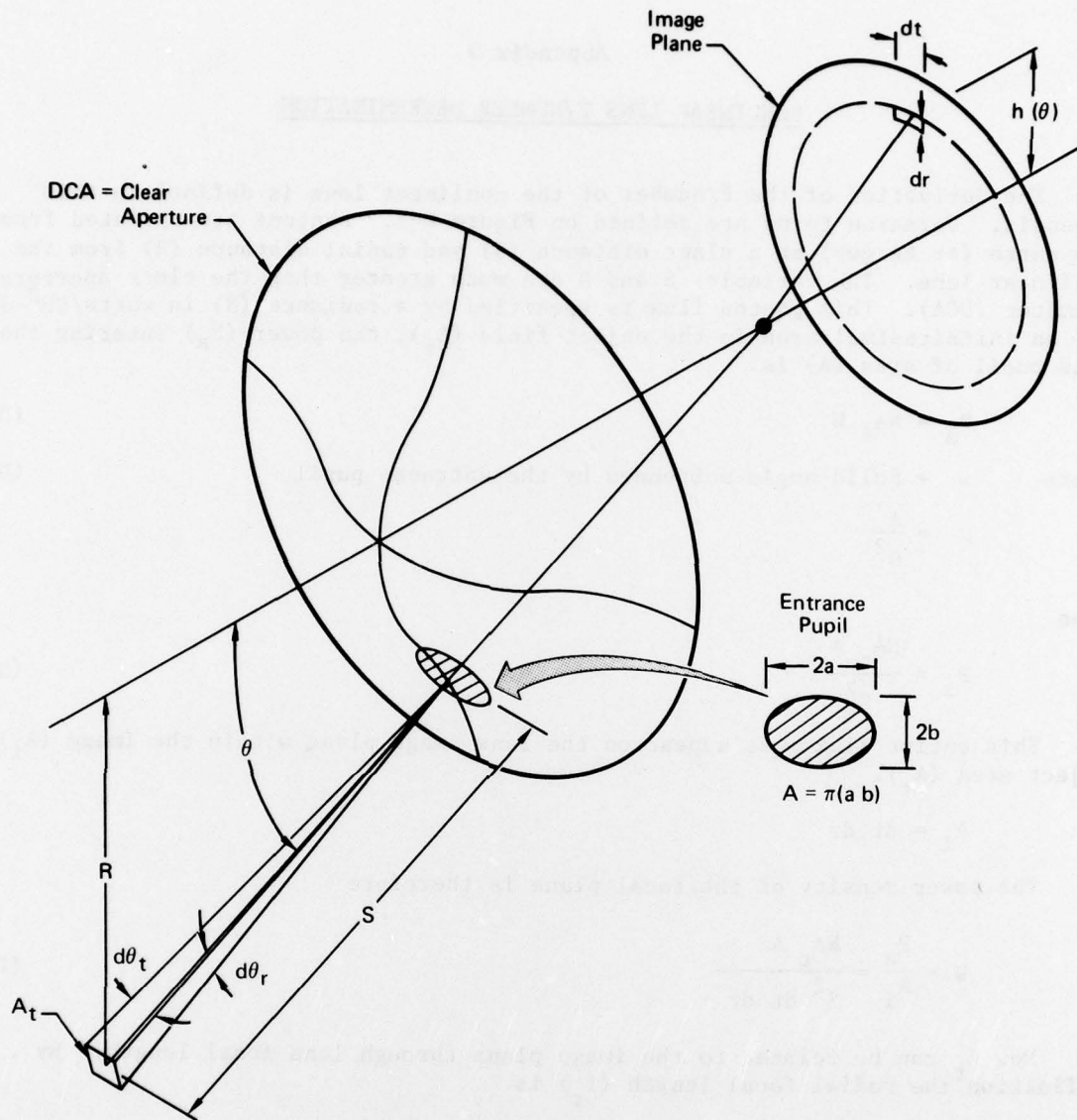
and the tangential focal length (f_t) is

$$f_t(\theta) = \frac{dt}{d\theta_t} \qquad (D-6)$$

where θ_r and θ_t are the radial and tangential angular subtense of A_t. Therefore,

$$dr = f_r(\theta)d(\theta_r) \qquad (D-7)$$

$$dt = f_t(\theta)d(\theta_t) \qquad (D-8)$$

Now $A_t = Sd\theta_r \cdot Sd\theta_t = S^2 d\theta_r d\theta_t \qquad$ (D-9)

FIGURE D-1
NONLINEAR LENS F/NUMBER DETERMINATION FROM ENTRANCE PUPIL SIZE

GP77-0328-12

Substituting this into Equation (D-4) we have

$$W = \frac{N A \frac{d\theta_r}{dt}\frac{d\theta_t}{dr}}{}$$ (D-10)

Now substituting Equation (D-8) and (D-9) into (D-10)

$$W = \frac{N A}{f_r(\theta)f_t(\theta)}$$ (D-11)

The focal length $f_r(\theta)$ is available from the original image height function used in lens design in the form of $h(\theta)$ vs θ, thus

$$f_r(\theta) = \frac{dh(\theta)}{d\theta}$$ (D-12)

The tangential focal length is not so obvious. It must be calculated by circular symmetry considerations. The same number of area elements must exist around the object field circumference $2\pi R$ as exist around the image plane circumference $2\pi\, h(\theta)$. In the object field the number of elements is:

$$N_{eo} = \frac{2\pi R}{d\theta_t S} = \frac{2\pi\, \text{Sin}\ \theta}{d\theta_t}$$ (D-13)

In the image plane the number of elements is

$$N_{ei} = \frac{2\pi h(\theta)}{dt}$$ (D-14)

Then Equation (D-13) and (D-14) may be set equal to each other

$$\frac{\text{Sin}\theta}{d\theta_t} = \frac{h(\theta)}{dt}$$ (D-15)

Or by definition of the focal length

$$f_t(\theta) = \frac{dt}{d\theta_t} = \frac{h(\theta)}{\text{Sin}\theta}$$ (D-16)

Substituting into Equation (D-11)

$$W = \frac{N A\, \text{Sin}\theta}{f_r(\theta)\ h(\theta)}$$ (D-17)

This expression can be evaluated over the image plane as a function of θ to determine uniformity of focal plane illumination (W). If the pupil is elliptical the area A is:

$$A = \pi ab$$ (D-18)

Equation (D-17) then becomes

$$W = \frac{N\pi ab\, \text{Sin}\ \theta}{f_r(\theta)h(\theta)}$$ (D-19)

67

To put this in relative terms, we can refer to the equivalent F/number of the nonlinear lens, i.e., the circular aperture F/number for a conventional lens that yields the same focal plane illumination as Equation (D-19).

If A was circular with diameter (D) and focal length constant (f) the flux through A would be

$$P_a = NA_t \frac{A}{s^2}$$ (D-20)

where

$$A = \frac{\pi D^2}{4}$$

then

$$P = \frac{N\pi D^2 A_t}{4s^2}$$ (D-21)

If the lens is conventional, all this power falls on an image area

$$A_i = A_t \frac{f^2}{s^2}$$

Therefore,

$$W = \frac{P}{A_i} = \frac{N\pi D^2}{4f^2} = \frac{N\pi}{4(F_{NOE})^2}$$

Equating this to Equation (D-19) and solving for F_{NOE}

$$F_{NOE} = \frac{1}{2} \sqrt{\frac{f_r(\theta)h(\theta)}{abSin\theta}}$$ (D-22)

This equation gives the nonlinear lens F/number in conventional terms. It is used to assess F/number uniformity of the nonlinear lens designs.

68

REFERENCES

1. Helmick, R. D., Fisher, R. W., Licis, G.; <u>A Non-Linear Lens for Bandwidth Reduction in Military TV System Applications</u>, Contract No. N00014-73-C-0154, 12 November 1973, Office of Naval Research, Arlington, VA 22217.

2. Remote Viewing System, Contract No. N00014-75-C-0660 Office of Naval Research, Arlington, VA 22217.

3. Fisher, R. W., et al, <u>Formal Lens Feasibility Study, 8-14 Microns Spectral Region, Final Report</u>, to be published under Contract No. N00014-76-C-0699 Office of Naval Research, Arlington, VA 22217.

4. Ratches, James, et al, <u>Night Vision Laboratory Static Performance Model For Thermal Viewing Systems</u>, Army Electronics Cmd., Fort Monmouth, NJ, Report No. 7043, April 1975.

B-1 Lloyd, J. M., <u>Thermal Imaging Systems</u>, Plenum Press, New York 1975